Geochemistry, Geophysics, Geosystems®

RESEARCH ARTICLE
10.1029/2021GC010200

**Key Points:**

- We build an open-system box model for kinetic clumped isotope effects (KIEs) in the $CaCO_3$-DIC-$H_2O$ system
- The model reproduces extreme $\delta^{18}O$ and $\Delta_{47}$ KIEs in high-pH inorganic calcite precipitation experiments
- The model can be adapted to investigate KIEs in natural carbonates, particularly if the dissolved inorganic carbon fluxes are constrained

**Supporting Information:**

Supporting Information may be found in the online version of this article.

**Correspondence to:**

J. M. Watkins,
watkins4@uoregon.edu

**Citation:**

Watkins, J. M., & Devriendt, L. S. (2022). A combined model for kinetic clumped isotope effects in the $CaCO_3$-DIC-$H_2O$ system. *Geochemistry, Geophysics, Geosystems*, *23*, e2021GC010200. https://doi.org/10.1029/2021GC010200

Received 6 OCT 2021
Accepted 7 MAY 2022

**Author Contributions:**

**Conceptualization:** James M. Watkins, Laurent S. Devriendt
**Funding acquisition:** James M. Watkins
**Investigation:** James M. Watkins, Laurent S. Devriendt
**Methodology:** James M. Watkins, Laurent S. Devriendt
**Project Administration:** James M. Watkins
**Resources:** James M. Watkins, Laurent S. Devriendt
**Software:** James M. Watkins
**Supervision:** James M. Watkins
**Validation:** James M. Watkins
**Visualization:** James M. Watkins
**Writing – original draft:** James M. Watkins



# A Combined Model for Kinetic Clumped Isotope Effects in the $CaCO_3$-DIC-$H_2O$ System

**James M. Watkins[1] and Laurent S. Devriendt[1,2]**

[1]Department of Earth Sciences, University of Oregon, Eugene, OR, USA, [2]Department of Ocean Systems, Royal Netherlands Institute for Sea Research (NIOZ), Utrecht University, Texel, The Netherlands

**Abstract** Most Earth surface carbonates precipitate out of isotopic equilibrium with their host solution, complicating the use of stable isotopes in paleoenvironment reconstructions. Disequilibrium can arise from exchange reactions in the DIC-$H_2O$ system as well as during crystal growth reactions in the DIC-$CaCO_3$ system. Existing models account for kinetic isotope effects (KIEs) in these systems separately but the models have yet to be combined in a general framework. Here, an open-system box model is developed for describing disequilibrium carbon, oxygen, and clumped ($\Delta_{47}$, $\Delta_{48}$, and $\Delta_{49}$) isotope effects in the $CaCO_3$-DIC-$H_2O$ system. The model is used to simulate calcite precipitation experiments in which the fluxes and isotopic compositions of $CO_2$ and $CaCO_3$ were constrained. Using a literature compilation of equilibrium and kinetic fractionation factors, modeled $\delta^{18}O$ and $\Delta_{47}$ values of calcite are in good agreement with the experimental data covering a wide range in crystal growth rate and solution pH. This relatively straightforward example provides a foundation for adapting the model to other situations involving $CO_2$ absorption (e.g., corals, foraminifera, and high-pH travertines) or degassing (e.g., speleothems, low-pH travertines, and cryogenic carbonates) and/or mixing with other dissolved inorganic carbon sources.

**Plain Language Summary** The clumped isotope composition ($\Delta_{47}$) of carbonate minerals is a measurement that can be used to determine the temperature of mineral formation. Sometimes, the inferred temperatures show systematic departures from expected temperatures, indicating that $\Delta_{47}$ holds additional information about the conditions of mineral growth. Our ability to extract this information is limited by an incomplete knowledge of how different steps in the crystallization process contribute to the net $\Delta_{47}$ value. This study develops a framework, informed by recent theoretical developments as well as data from carbonates grown under controlled settings, for interpreting the $\Delta_{47}$ of carbonate minerals when temperature is not the only controlling factor.

## 1. Introduction

The carbon, oxygen, and clumped isotope compositions of carbonate minerals are widely used for paleoenvironment reconstructions. When crystals grow slowly, near equilibrium, oxygen isotope partitioning and bond ordering (e.g., $^{13}C$-$^{18}O$, $^{18}O$-$^{18}O$, and $^{13}C$-$^{18}O$-$^{18}O$) are expected to depend solely on temperature (Bigeleisen & Mayer, 1947; Eiler, 2007; Ghosh et al., 2006; Urey, 1947). Natural mineral growth, however, typically occurs under nonequilibrium conditions (Coplen, 2007; Daëron et al., 2019; Kluge et al., 2014), as does precipitation of calcite in laboratory experiments (Affek & Zaarur, 2014; Dietzel et al., 2009; Gabitov et al., 2012; Kim & O'Neil, 1997; Watkins et al., 2013). The resulting kinetic isotope effects (KIEs) can arise from multiple processes, including but not limited to: (a) diffusive transport of $CO_2$ through membranes (Hansen et al., 2017; Thiagarajan et al., 2011), (b) crystal growth reactions (DePaolo, 2011; Watkins et al., 2013), and (c) isotope exchange reactions between dissolved inorganic carbon species (DIC = $CO_2 + HCO_3^- + CO_3^{2-}$) and water (e.g., Affek, 2013; Bajnai et al., 2018; Devriendt et al., 2017a; Guo, 2008; Staudigel & Swart, 2018; Uchikawa & Zeebe, 2012; Usdowski et al., 1991; Zeebe & Wolf-Gladrow, 2001; many others). Reconstructing environments from disequilibrium isotope compositions requires knowledge of the reaction pathways and the KIEs that arise during each step in mineral formation.

Over the past decade, significant progress has been made toward quantifying KIEs in the $CaCO_3$-DIC-$H_2O$ system (Figure 1). In the simplest scenario of $CaCO_3$ growth from an isotopically equilibrated DIC pool, KIEs can be attributed to the following crystal growth reactions (Watkins et al., 2013):

$$Ca^{2+} + CO_3^{2-} \underset{\nu_{B_1}}{\overset{k_{B_1}}{\rightleftharpoons}} CaCO_3, \quad (1)$$

**Writing – review & editing:** James M. Watkins, Laurent S. Devriendt

and

$$Ca^{2+} + HCO_3^- \underset{\nu_{B_2}}{\overset{k_{B_2}}{\rightleftharpoons}} CaCO_3 + H^+ \quad (2)$$

where the $k'$s and $\nu'$s are mass-dependent rate constants following the notation of Wolthers et al. (2012). For calcite, the KIEs attending these reactions can be significant across the full range of growth rate and pH: ~1–4‰ for $\delta^{18}O$ and ~0.03‰ for $\Delta_{47}$ (Watkins & Hunt, 2015; Watkins et al., 2014), which translate to $\Delta T$ of about 4–16°C and 7–11°C, respectively (Ghosh et al., 2006; McCrea, 1950; Zaarur et al., 2013). Although this is a fairly large temperature range, the temperature sensitivities of most empirical calibrations are probably not compromised by surface reaction-controlled KIEs because each individual $CaCO_3$ archive forms within a relatively narrow range in mineral growth rate and pH. It is clear, however, that different $CaCO_3$ archives are recorded at different precipitation rates, contributing to archive-specific isotopic offsets from the established inorganic calibrations (e.g., Candelier et al., 2013; Dennis & Schrag, 2010; Devriendt et al., 2017b; Ghosh et al., 2006; Kele et al., 2015; Kelson et al., 2017; Kim & O'Neil, 1997; Kluge et al., 2015; Marchitto et al., 2014; McCrea, 1950; O'Neil et al., 1969; Parker et al., 2017; Watkins et al., 2013; Zaarur et al., 2013, and many others).

The situation is more complex when $CaCO_3$ precipitates from a DIC pool that is not isotopically equilibrated. Here, the key reactions are the relatively slow $CO_2$ (de-)hydration and (de-)hydroxylation reactions:

$$CO_2 + H_2O \underset{k_{-1}}{\overset{k_{+1}}{\rightleftharpoons}} HCO_3^- + H^+ \quad (3)$$

and

$$CO_2 + OH^- \underset{k_{-4}}{\overset{k_{+4}}{\rightleftharpoons}} HCO_3^-, \quad (4)$$

where the $k'$s are isotopologue-specific rate constants. If the reactions are unidirectional (either forward or backward), the KIEs can be an order of magnitude larger than those attending crystal growth (Christensen et al., 2021; Clark & Fontes, 1990; Clark et al., 1992; Devriendt et al., 2017a; Falk et al., 2016; Guo, 2008, 2020; Guo et al., 2009; Leleu et al., 2016; Mervine et al., 2014; O'Neil & Barnes, 1971; Yumol et al., 2020). More often than not, however, these reactions are bidirectional, and an important objective is to be able to estimate the degree of reaction reversibility and the net magnitude of KIEs.

Two different approaches have been taken to model KIEs in the DIC-$H_2O$ system in the absence of crystal growth. The IsoDIC model of Guo (2020) tracks all of the reactions ($n$ = 155) involving $^{12}C$, $^{13}C$, $^{16}O$, $^{17}O$, and $^{18}O$. This amounts to 32 coupled ordinary differential equations (ODEs) describing changes in the concentration of $CO_2$ and $HCO_3^-$ isotopologues (Table 1). By contrast, the ExClump38 model of Uchikawa et al. (2021) only tracks the major isotopologue at each mass, up to mass 63 (Table 1). The latter approach has the advantage of only requiring 8 ODEs for clumped isotopes (i.e., $\Delta_{47}$) but it includes approximations that have not been fully explained or validated against the IsoDIC model. Additionally, the ExClump38 model does not include $^{18}O$-$^{18}O$ ($\Delta_{48}$) and $^{13}C$-$^{18}O$-$^{18}O$ ($\Delta_{49}$) isotopologues.

In this contribution, we build upon existing $CaCO_3$-DIC and DIC-$H_2O$ models by deriving the equations for $^{18}O$-$^{18}O$ and $^{13}C$-$^{18}O$-$^{18}O$ clumped isotopes. The two complementary models are merged together in a box model framework that can describe kinetic clumped isotope effects in the full $CaCO_3$-DIC-$H_2O$ system. The model was applied with oxygen and carbon kinetic and equilibrium fractionation factors (KFFs and EFFs) compiled from previously published laboratory or field studies and clumped isotope KFFs and EFFs taken from the theoretical work of Guo (2020). We refer to the combined model using the acronym "COAD," which stands for "carbon, oxygen, $\alpha$, $\Delta$." We provide the first application of the COAD box model to $\delta^{18}O$ and $^{13}C$-$^{18}O$ clumped isotope measurements from calcite precipitation experiments where there is a known $CO_2$ influx and $CaCO_3$ outflux. The example provided can be extended to future $^{18}O$-$^{18}O$ and $^{13}C$-$^{18}O$-$^{18}O$ clumped isotope measurements and modified to describe KIEs attending carbonate precipitation in other settings.

## 2. Definitions, Notation, and Guides

The $CaCO_3$-DIC and DIC-$H_2O$ models track the concentrations of isotopologues. The studies upon which these models are based use different notation, which can be a source of confusion. In this study, we have made our

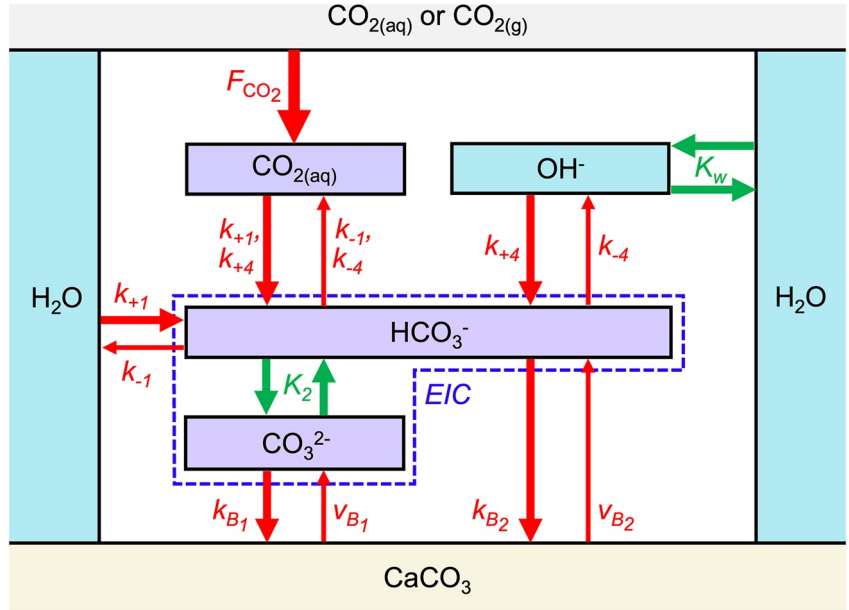


**Figure 1.** Overview of the chemical species and reactions considered herein. Kinetic isotope fractionation for carbon, oxygen, and clumped isotopes are recorded in $CaCO_3$ where there is one or more reaction(s) involving a dissolved inorganic carbon species (DIC = $CO_{2(aq)} + HCO_3^- + CO_3^{2-}$; purple boxes) with backward/forward rate ratio(s) not equal to unity (red arrows: $CO_2$ hydration/hydroxylation and $HCO_3^-$ dehydration/dehydroxylation; attachment/detachment of $CO_3^{2-}$ and $HCO_3^-$ to/from $CaCO_3$). Reactions that are several orders of magnitude faster than the $CO_2$ hydration/hydroxylation and $CaCO_3$ precipitation/dissolution reactions are assumed to reach chemical and isotopic equilibrium (green arrows: $OH^-$ protonation and $H_2O$ deprotonation; $CO_3^{2-}$ protonation and $HCO_3^-$ deprotonation). The species $CO_3^{2-}$ and $HCO_3^-$ are always in isotopic equilibrium with one another and form the equilibrated inorganic carbon pool (EIC) while $CO_{2(aq)}$ is not always in isotopic equilibrium with the EIC. The kinetics of isotope exchange between the EIC and $H_2O$ depends on the rate of the $CO_2$ hydration/hydroxylation reactions, which positively covary with the $CO_{2(aq)}$/EIC concentration ratio. In most cases, the isotopic composition of $CaCO_3$ is a convolution of equilibrium and kinetic isotope fractionations in the $CaCO_3$-DIC-$H_2O$ system.

best effort to adopt a notation that is self-consistent while being compatible with previous studies. Since the $CaCO_3$-DIC and DIC-$H_2O$ models rely on conversions between isotope ratios ($r$) and isotopologue ratios ($R$), this section is intended to serve as a stand-alone reference for these conversions and how they are implemented in clumped isotope calculations.

### 2.1. Equilibrium and Kinetic Fractionation Factors

Equilibrium and nonequilibrium fractionation factors are written in the following form:

$$^{18}\alpha_{CaCO_3-H_2O} = \frac{^{18}r_{CaCO_3}}{^{18}r_{H_2O}} = \frac{\left(\frac{^{18}O}{^{16}O}\right)_{CaCO_3}}{\left(\frac{^{18}O}{^{16}O}\right)_{H_2O}}, \quad (5)$$

where subscripts on $\alpha$ direct the reader to the relevant phases or chemical species. When referring to an equilibrium $\alpha$ or $r$, we append a superscript "eq" (e.g., $^{18}\alpha^{eq}_{CaCO_3-H_2O}$).

Kinetic fractionation factors (KFFs) are associated with kinetic limits during unidirectional reactions and are defined as the ratio of isotope-specific rate constants. For example, the oxygen isotope KFFs attending the forward (crystal growth) reactions (reactions 1 and 2) are given by

$$^{18}\alpha^{kin}_{k_{B_1}} = \frac{^{18}k_{B_1}}{^{16}k_{B_1}} \quad (6)$$

**Table 1**
*List of $CO_2$ and $HCO_3^-$ or $CO_3^{2-}$ Isotopologues Tracked in the IsoDIC Model of Guo (2020)*

| Number ID | Isotopologue | Mass (ignoring H) | Permutations | Abundance |
|---|---|---|---|---|
| *Part I:* $CO_2$ | | | | |
| 1 | **$^{12}C^{16}O^{16}O$** | **44** | 1 | 98.40% |
| 2 | **$^{13}C^{16}O^{16}O$** | **45** | 1 | 1.11% |
| 3 | $^{12}C^{17}O^{16}O$ | 45 | 2 | 748 ppm |
| 4 | **$^{12}C^{18}O^{16}O$** | **46** | 2 | 0.40% |
| 5 | $^{13}C^{17}O^{16}O$ | 46 | 2 | 8.4 ppm |
| 6 | $^{12}C^{17}O^{17}O$ | 46 | 1 | 0.142 ppm |
| 7 | **$^{13}C^{18}O^{16}O$** | **47** | 2 | 44.4 ppm |
| 8 | $^{12}C^{17}O^{18}O$ | 47 | 2 | 1.50 ppm |
| 9 | $^{13}C^{17}O^{17}O$ | 47 | 1 | 1.60 ppb |
| 10 | **$^{12}C^{18}O^{18}O$** | **48** | 1 | 3.96 ppm |
| 11 | $^{13}C^{17}O^{18}O$ | 48 | 2 | 16.8 ppb |
| 12 | **$^{13}C^{18}O^{18}O$** | **49** | 1 | 44.5 ppb |
| | | | | 100.0% |
| *Part II:* $HCO_3^-$ *or* $CO_3^{2-}$ | | | | |
| 1 | **$H^{12}C^{16}O^{16}O^{16}O$** | **60** | 1 | 98.20% |
| 2 | **$H^{13}C^{16}O^{16}O^{16}O$** | **61** | 1 | 1.10% |
| 3 | $H^{12}C^{17}O^{16}O^{16}O$ | 61 | 3 | 0.11% |
| 4 | **$H^{12}C^{18}O^{16}O^{16}O$** | **62** | 3 | 0.60% |
| 5 | $H^{13}C^{17}O^{16}O^{16}O$ | 62 | 3 | 12 ppm |
| 6 | $H^{12}C^{17}O^{17}O^{16}O$ | 62 | 3 | 405 ppb |
| 7 | **$H^{13}C^{18}O^{16}O^{16}O$** | **63** | 3 | 67 ppm |
| 8 | $H^{12}C^{17}O^{18}O^{16}O$ | 63 | 6 | 4.4 ppm |
| 9 | $H^{13}C^{17}O^{17}O^{16}O$ | 63 | 3 | 4.54 ppb |
| 10 | $H^{12}C^{17}O^{17}O^{17}O$ | 63 | 1 | 50 ppt |
| 11 | **$H^{12}C^{18}O^{18}O^{16}O$** | **64** | 3 | 12 ppm |
| 12 | $H^{13}C^{17}O^{18}O^{16}O$ | 64 | 6 | 50 ppb |
| 13 | $H^{12}C^{17}O^{17}O^{18}O$ | 64 | 3 | 828 ppt |
| 14 | $H^{13}C^{17}O^{17}O^{17}O$ | 64 | 1 | 0.5 ppt |
| 15 | **$H^{13}C^{18}O^{18}O^{16}O$** | **65** | 3 | 138 ppb |
| 16 | $H^{12}C^{17}O^{18}O^{18}O$ | 65 | 3 | 4.5 ppb |
| 17 | $H^{13}C^{17}O^{17}O^{18}O$ | 65 | 3 | 9 ppt |
| 18 | $H^{12}C^{18}O^{18}O^{18}O$ | 66 | 1 | 8 ppb |
| 19 | $H^{13}C^{17}O^{18}O^{18}O$ | 66 | 3 | 51 ppt |
| 20 | $H^{13}C^{18}O^{18}O^{18}O$ | 67 | 1 | 94 ppt |
| | | | | 100.0% |

*Note*. The subset of isotopologues in bold are tracked in the model presented herein. Abundances are from Eiler (2007) and Ghosh et al. (2006).

and

$$^{18}\alpha^{\text{kin}}_{k_{B_2}} = \frac{^{18}k_{B_2}}{^{16}k_{B_2}}, \tag{7}$$

where subscripts on $\alpha$ direct the reader to the relevant reaction and the "kin" superscripts make clear that these are KFFs.

### 2.2. "Cheat Sheet" for Conversions Between Isotope Ratios and Isotopologue Ratios

In the case where the isotopes are randomly distributed, we have the following relationships for oxygen isotopes in $CO_3^{2-}$ (note that C refers to $^{12}C + {}^{13}C$):

$$\left[C^{16}O^{16}O^{16}O\right] = P(16,16,16) = (0.998)^3 \approx 0.994 \tag{8}$$

$$\left[C^{16}O^{16}O^{18}O\right] = P(16,16,18) = 3(0.998)(0.998)(0.002) \approx 0.005998 \tag{9}$$

$$\left[C^{16}O^{18}O^{18}O\right] = P(16,18,18) = 3(0.998)(0.002)(0.002) \approx 0.000012 \tag{10}$$

and

$$\left[C^{18}O^{18}O^{18}O\right] = P(18,18,18) = (0.002)^3 \approx 8 \times 10^{-9}, \tag{11}$$

where in this example $^{18}O$ constitutes 2% of oxygen atoms in $CO_3^{2-}$ and the $P$'s refer to probabilities. Without rounding, the values sum to exactly 1. The $^{18}O/^{16}O$ ratio of $CO_3^{2-}$ is related to the isotopologue abundances through

$$\begin{aligned} ^{18}r_{CO_3^{2-}} &= \left(\frac{^{18}O}{^{16}O}\right)_{CO_3^{2-}} \\ &= \frac{\left[C^{16}O^{16}O^{18}O\right] + 2\left[C^{16}O^{18}O^{18}O\right] + 3\left[C^{18}O^{18}O^{18}O\right]}{3\left[C^{16}O^{16}O^{16}O\right] + 2\left[C^{16}O^{16}O^{18}O\right] + \left[C^{16}O^{18}O^{18}O\right]}. \end{aligned} \tag{12}$$

Equation 12 is exact in all cases. In the case of a stochastic distribution, the $^{18}O/^{16}O$ ratio can be expressed using any two different isotopologues without losing any information (i.e., each of the following expressions returns the exact $^{18}O/^{16}O$ ratio):

$$^{18}r_{CO_3^{2-}} = \left(\frac{\left[C^{18}O^{18}O^{18}O\right]}{\left[C^{16}O^{16}O^{16}O\right]}\right)^{1/3} = \left(\frac{(0.002)(0.002)(0.002)}{(0.998)(0.998)(0.998)}\right)^{1/3}, \tag{13}$$

or

$$^{18}r_{CO_3^{2-}} = \frac{1}{3}\frac{\left[C^{16}O^{16}O^{18}O\right]}{\left[C^{16}O^{16}O^{16}O\right]} = \frac{3(0.998)(0.998)(0.002)}{3(0.998)(0.998)(0.998)}, \tag{14}$$

or

$$^{18}r_{CO_3^{2-}} = \left(\frac{\left[C^{16}O^{18}O^{18}O\right]}{3\left[C^{16}O^{16}O^{16}O\right]}\right)^{1/2} = \left(\frac{3(0.998)(0.002)(0.002)}{3(0.998)(0.998)(0.998)}\right)^{1/2}. \tag{15}$$

Because the singly substituted isotopologue is the second most abundant, a sensible choice is to use Equation 14 as done by Watkins et al. (2014) in their ion-by-ion model for calcite growth from $HCO_3^-$ and $CO_3^{2-}$ isotopologues.

For $CO_2$, we have:

$$\left[C^{16}O^{16}O\right] = P(16,16) = (0.998)^2 \approx 0.996 \tag{16}$$

$$\left[C^{16}O^{18}O\right] = P(16,18) = 2(0.998)(0.002) \approx 0.003992 \tag{17}$$

$$\left[C^{18}O^{18}O\right] = P(18,18) = (0.002)^2 \approx 4 \times 10^{-6} \tag{18}$$

The $^{18}O/^{16}O$ ratio can be written as:

$$^{18}r_{CO_2} = \left(\frac{^{18}O}{^{16}O}\right)_{CO_2} = \frac{\left[C^{16}O^{18}O\right] + 2\left[C^{18}O^{18}O\right]}{2\left[C^{16}O^{16}O\right] + \left[C^{16}O^{18}O\right]}. \tag{19}$$

There are two other ways this can be written:

$$^{18}r_{CO_2} = \left(\frac{\left[C^{18}O^{18}O\right]}{\left[C^{16}O^{16}O\right]}\right)^{1/2} = \left(\frac{(0.002)(0.002)}{(0.998)(0.998)}\right)^{1/2} \tag{20}$$

or

$$^{18}r_{CO_2} = \frac{1}{2}\frac{\left[C^{16}O^{18}O\right]}{\left[C^{16}O^{16}O\right]} = \frac{2(0.002)(0.998)}{2(0.998)(0.998)}. \tag{21}$$

In this study, we express carbon and oxygen isotope compositions and equilibrium fractionation factors in a self-consistent way using the abundance ratios of singly and non-substituted isotopologues (Equations 14 and 21).

### 2.3. Shorthand Notation

For isotopologues, we hereafter use the following shorthand notation: $^{12}C = 2$, $^{13}C = 3$, $^{16}O = 6$, and $^{18}O = 8$. We also drop the superscript charges on ionic species (e.g., $[H^+]$ becomes [H] and $[H2666^-]$ becomes [H2666]) unless the species are used in the subscript to a fractionation factor (e.g., $^{18}\alpha_{HCO_3^- - H_2O}$). We treat permutations (e.g., 286–268) and isotopomers (e.g., 2886-2868-2688) as indistinguishable such that [2886] refers to the total concentration of doubly substituted $CO_3^{2-}$; that is, [2886] = [2886] + [2868] + [2688].

### 2.4. Equilibrium Clumped Isotopes

#### 2.4.1. $^{13}C$-$^{18}O$ Clumped Isotopes

Clumped isotope thermometry involves the equilibrium of $^{13}C$-$^{18}O$ bonding within a single species. For $CO_2$, we can write the following isotope exchange reaction:

$$366 + 286 \rightleftharpoons 386 + 266, \tag{22}$$

which has an equilibrium constant

$$^{47}K_{CO_2} = \frac{[386][266]}{[366][286]}. \tag{23}$$

The abundance of 386 is measured as (Eiler, 2007):

$$\Delta_{47} = \left[\left(\frac{^{47}R}{^{47}R^*} - 1\right) - \left(\frac{^{46}R}{^{46}R^*} - 1\right) - \left(\frac{^{45}R}{^{45}R^*} - 1\right)\right] \times 1000, \tag{24}$$

where $^{47}R$, $^{46}R$, and $^{45}R$ are the abundance ratios of masses 47, 46, and 45 relative to mass 44, and the asterisk denotes the stochastic distribution. The $^{46}R$ and $^{45}R$ terms in Equation 24 depend on $^{17}r_{CO_2}$, which cannot be measured independently due to mass interferences between $^{17}O$ and $^{13}C$. $^{17}r_{CO_2}$ is commonly estimated from $^{18}r_{CO_2}$ and

assuming a $^{17}O/^{18}O$ natural abundance ratio. The result of this should lead to $^{46}R = {}^{46}R^*$ and $^{45}R = {}^{45}R^*$, in which case Equation 24 simplifies to (Eiler & Schauble, 2004; Saenger et al., 2021):

$$\Delta_{47} = \left(\frac{{}^{47}R}{{}^{47}R^*} - 1\right) \times 1000, \tag{25}$$

where

$${}^{47}R = \frac{[386]}{[266]}. \tag{26}$$

The stochastic ratio, ${}^{47}R^*$, can be calculated from the carbon and oxygen isotope composition, and ${}^{47}K_{CO_2}$ can be related to $\Delta_{47}$ values by first multiplying the top and bottom by [266]:

$${}^{47}K_{CO_2} = \frac{[386]}{[266]}\frac{[266]}{[366]}\frac{[266]}{[286]} = {}^{47}R \cdot \underbrace{\left({}^{13}r_{CO_2}\right)^{-1} \cdot \left(2 \cdot {}^{18}r_{CO_2}\right)^{-1}}_{{}^{47}R^{*-1}} = \left(\frac{{}^{47}R}{{}^{47}R^*}\right)^{eq}_{CO_2}. \tag{27}$$

Here, the equilibrium constant $K$ is equivalent to $R/R^*$. As shown below, however, this is not the case for $^{18}O$-$^{18}O$ and $^{13}C$-$^{18}O$-$^{18}O$ clumped isotopes. Combining Equation 25 with Equation 27 leads to

$${}^{47}K_{CO_2} = \left(\frac{{}^{47}R}{{}^{47}R^*}\right)^{eq}_{CO_2} = \frac{[386][266]}{[366][286]} = \left(\frac{\Delta^{eq}_{47,CO_2}}{1000} + 1\right). \tag{28}$$

Similar expressions can be written for clumped isotope equilibrium in $HCO_3^-$ and $CO_3^{2-}$:

$$H3666 + H2866 \rightleftharpoons H3866 + H2666 \tag{29}$$

and

$$3666 + 2866 \rightleftharpoons 3866 + 2666, \tag{30}$$

which have equilibrium constants

$${}^{63}K_{HCO_3^-} = \frac{[H3866][H2666]}{[H3666][H2866]} = \left(\frac{{}^{63}R}{{}^{63}R^*}\right)^{eq}_{HCO_3^-} = \left(\frac{\Delta^{eq}_{63,HCO_3^-}}{1000} + 1\right) \tag{31}$$

and

$${}^{63}K_{CO_3^{2-}} = \frac{[3866][2666]}{[3666][2866]} = \left(\frac{{}^{63}R}{{}^{63}R^*}\right)^{eq}_{CO_3^{2-}} = \left(\frac{\Delta^{eq}_{63,CO_3^{2-}}}{1000} + 1\right). \tag{32}$$

### 2.4.2. $^{18}O$-$^{18}O$ Clumped Isotopes

The mass 48 and 64 isotopologues involve $^{18}O$-$^{18}O$ clumps. For $CO_2$, we can write the following isotope exchange reaction:

$$286 + 286 \rightleftharpoons 288 + 266 \tag{33}$$

which has an equilibrium constant

$${}^{48}K_{CO_2} = \frac{[288][266]}{[286][286]}. \tag{34}$$

The abundance of 288 is measured as:

$$\Delta_{48} = \left(\frac{{}^{48}R}{{}^{48}R^*} - 1\right) \times 1000, \tag{35}$$

where

$$^{48}R = \frac{[288]}{[266]}. \tag{36}$$

Unlike the case for $^{13}C$-$^{18}O$ clumped isotopes, the $^{48}K_{CO_2}$ and $R/R^*$ are not equivalent:

$$^{48}K_{CO_2} = \frac{[288]}{[266]}\frac{[266]}{[286]}\frac{[266]}{[286]} = {}^{48}R \cdot \left(2 \cdot {}^{18}r_{CO_2}\right)^{-1} \cdot \left(2 \cdot {}^{18}r_{CO_2}\right)^{-1} = \frac{1}{4}\left(\frac{^{48}R}{^{48}R^*}\right)^{eq}_{CO_2}, \tag{37}$$

where we have used the relationship from Section 2.2 (Equation 20) that, for a stochastic distribution,

$$^{48}R^* = \left(\frac{[288]}{[266]}\right)^* = {}^{18}r^2_{CO_2}. \tag{38}$$

The factor of 1/4 in Equation 37 will be important in the derivation of backward rate constants for dehydration and dehydroxylation.

Combining Equation 35 with Equation 37 leads to

$$^{48}K_{CO_2} = \frac{[288][266]}{[286][286]} = \frac{1}{4}\left(\frac{^{48}R}{^{48}R^*}\right)^{eq}_{CO_2} = \frac{1}{4}\left(\frac{\Delta^{eq}_{48,CO_2}}{1000} + 1\right). \tag{39}$$

Similar expressions can be written for clumped isotope equilibrium in $HCO_3^-$ and $CO_3^{2-}$:

$$\mathrm{H2866} + \mathrm{H2866} \rightleftharpoons \mathrm{H2886} + \mathrm{H2666} \tag{40}$$

and

$$2866 + 2866 \rightleftharpoons 2886 + 2666, \tag{41}$$

which have equilibrium constants

$$^{64}K_{HCO_3^-} = \frac{[\mathrm{H2886}][\mathrm{H2666}]}{[\mathrm{H2866}][\mathrm{H2866}]} = \frac{1}{3}\left(\frac{^{64}R}{^{64}R^*}\right)^{eq}_{HCO_3^-} = \frac{1}{3}\left(\frac{\Delta^{eq}_{64,HCO_3^-}}{1000} + 1\right) \tag{42}$$

and

$$^{64}K_{CO_3^{2-}} = \frac{[2886][2666]}{[2866][2866]} = \frac{1}{3}\left(\frac{^{64}R}{^{64}R^*}\right)^{eq}_{CO_3^{2-}} = \frac{1}{3}\left(\frac{\Delta^{eq}_{64,CO_3^{2-}}}{1000} + 1\right). \tag{43}$$

#### 2.4.3. $^{13}C$-$^{18}O$-$^{18}O$ Clumped Isotopes

The mass 49 and 65 isotopologues involve $^{13}C$-$^{18}O$-$^{18}O$ clumps. For $CO_2$, we can write the following isotope exchange reaction:

$$386 + 286 \rightleftharpoons 388 + 266, \tag{44}$$

which has an equilibrium constant

$$^{49}K_{CO_2} = \frac{[388][266]}{[386][286]}. \tag{45}$$

The abundance of 388 is measured as:

$$\Delta_{49} = \left(\frac{^{49}R}{^{49}R^*} - 1\right) \times 1000, \tag{46}$$

where

$$^{49}R = \frac{[388]}{[266]}. \tag{47}$$

By multiplying the top and bottom by [266] we have:

$$^{49}K_{CO_2} = \frac{[388]}{[266]}\frac{[266]}{[386]}\frac{[266]}{[286]}. \quad (48)$$

This expression involves the [386]/[266] ratio, which cannot be treated as stochastic. To get the non-stochastic ratio, recall from Section 2.2 that for a stochastic distribution, we have

$$^{47}R^* = \left(\frac{[386]}{[266]}\right)^* = \frac{[366]}{[266]} \cdot \frac{[286]}{[266]} = {}^{13}r_{CO_2} \cdot 2 \cdot {}^{18}r_{CO_2}, \quad (49)$$

which is used to express the non-stochastic $^{47}R$ as follows:

$$^{47}R = \frac{[386]}{[266]} = \left(\frac{^{47}R}{^{47}R^*}\right) \cdot {}^{13}r_{CO_2} \cdot 2 \cdot {}^{18}r_{CO_2}. \quad (50)$$

This leads to an expression for $^{49}K_{CO_2}$ that depends on the $^{13}$C-$^{18}$O clumped isotope composition:

$$^{49}K_{CO_2} = \frac{[388]}{[266]}\frac{[266]}{[386]}\frac{[266]}{[286]} = {}^{49}R \cdot \left(\frac{^{47}R}{^{47}R^*}\right)^{-1} \cdot \left({}^{13}r_{CO_2}\right)^{-1} \cdot \left(2 \cdot {}^{18}r_{CO_2}\right)^{-1} \cdot \left(2 \cdot {}^{18}r_{CO_2}\right)^{-1} = \frac{\frac{1}{4}\left(\frac{^{49}R}{^{49}R^*}\right)^{eq}_{CO_2}}{\left(\frac{^{47}R}{^{47}R^*}\right)^{eq}_{CO_2}}, \quad (51)$$

which is similar to the analogous expression for the mass 48 and 64 isotopologues in that the factor of 1/4 comes from the oxygen isotope part of the expression. Combining Equation 46 with Equation 51 leads to

$$^{49}K_{CO_2} = \frac{[388][266]}{[386][286]} = \frac{\frac{1}{4}\left(\frac{^{49}R}{^{49}R^*}\right)^{eq}_{CO_2}}{\left(\frac{^{47}R}{^{47}R^*}\right)^{eq}_{CO_2}} = \frac{\frac{1}{4}\left(\frac{\Delta^{eq}_{49,CO_2}}{1000} + 1\right)}{\left(\frac{\Delta^{eq}_{47,CO_2}}{1000} + 1\right)}. \quad (52)$$

Similar expressions can be written for clumped isotope equilibrium in $HCO_3^-$ and $CO_3^{2-}$:

$$H3866 + H2866 \rightleftharpoons H3886 + H2666 \quad (53)$$

and

$$3866 + 2866 \rightleftharpoons 3886 + 2666, \quad (54)$$

which have equilibrium constants

$$^{65}K_{HCO_3^-} = \frac{[H3886][H2666]}{[H3866][H2866]} = \frac{\frac{1}{3}\left(\frac{^{65}R}{^{65}R^*}\right)^{eq}_{HCO_3^-}}{\left(\frac{^{63}R}{^{63}R^*}\right)^{eq}_{HCO_3^-}} = \frac{\frac{1}{3}\left(\frac{\Delta^{eq}_{65,HCO_3^-}}{1000} + 1\right)}{\left(\frac{\Delta^{eq}_{63,HCO_3^-}}{1000} + 1\right)} \quad (55)$$

and

$$^{65}K_{CO_3^{2-}} = \frac{[3886][2666]}{[3866][2866]} = \frac{\frac{1}{3}\left(\frac{^{65}R}{^{65}R^*}\right)^{eq}_{CO_3^{2-}}}{\left(\frac{^{63}R}{^{63}R^*}\right)^{eq}_{CO_3^{2-}}} = \frac{\frac{1}{3}\left(\frac{\Delta^{eq}_{65,CO_3^{2-}}}{1000} + 1\right)}{\left(\frac{\Delta^{eq}_{63,CO_3^{2-}}}{1000} + 1\right)}. \quad (56)$$

## 3. $CaCO_3$-DIC Model

Kinetic isotope fractionation arising from reactions (1) and (2) have been investigated by growing calcite from an isotopically equilibrated DIC pool and developing "ion-by-ion" models of crystal growth to describe the results (Levitt et al., 2018; Watkins & Hunt, 2015; Watkins et al., 2013, 2014; Wolthers et al., 2012). For clumped

isotopes, the latest version of the ion-by-ion model is limited to the mass 63 isotopologue of $CaCO_3$ (Watkins & Hunt, 2015), but there are good reasons to extend the model to heavier isotopologues. For example, despite the low abundance of the mass 64 isotopologue (Table 1), it is now possible to measure $\Delta_{48}$ with sufficient precision to resolve departures from equilibrium in $\Delta_{47}$-$\Delta_{48}$ (or $\Delta_{63}$-$\Delta_{64}$) space (Bajnai et al., 2020; Fiebig et al., 2019; Fiebig et al., 2021; Swart et al., 2021). Such measurements could potentially be used to correct for kinetic effects and infer temperatures of carbonate formation from samples that were previously thought to be compromised (Bajnai et al., 2020; Fiebig et al., 2021). New $\Delta_{48}$ measurements will also be useful for distinguishing between competing models of kinetic effects arising from various inorganic and biological processes (Guo, 2020). In this section, we present an updated compilation of data and fractionation factors for carbon, oxygen, and $^{13}C$-$^{18}O$ clumped isotopes, and then extend the ion-by-ion model to $^{18}O$-$^{18}O$ and $^{13}C$-$^{18}O$-$^{18}O$ clumped isotopes in anticipation of future applications.

### 3.1. Carbon and Oxygen Isotopes

In the ion-by-ion model, the nonequilibrium isotopic composition of calcite is a function of growth rate and pH through the attachment rates (AR) and detachment rates (DR) of the isotopologues of $HCO_3^-$ and $CO_3^{2-}$ during crystal growth. The equations for calculating the singly substituted carbon and oxygen isotopologue ratios of calcite are:

$$ {}^{13}R_{CaCO_3} = \frac{[Ca3666]}{[Ca2666]} = \frac{{}^{13}R^{eq}_{CaCO_3} \cdot AR}{\frac{{}^{13}R^{eq}_{CaCO_3}(AR-DR)}{(1-\chi)\cdot{}^{13}\alpha^{kin}_{k_{B_1}}\cdot{}^{13}R_{CO_3^{2-}} + \chi\cdot{}^{13}\alpha^{kin}_{k_{B_2}}\cdot{}^{13}R_{HCO_3^-}}} + DR, \quad (57) $$

and

$$ {}^{18}R_{CaCO_3} = \frac{[Ca2866]}{[Ca2666]} = \frac{{}^{18}R^{eq}_{CaCO_3} \cdot AR}{\frac{{}^{18}R^{eq}_{CaCO_3}(AR-DR)}{(1-\chi)\cdot{}^{18}\alpha^{kin}_{k_{B_1}}\cdot{}^{18}R_{CO_3^{2-}} + \chi\cdot{}^{18}\alpha^{kin}_{k_{B_2}}\cdot{}^{18}R_{HCO_3^-}}} + DR. \quad (58) $$

where $\chi$ is the fraction of $HCO_3^-$ in EIC (i.e., $[HCO_3^-]$ / ($[HCO_3^-]$ + $[CO_3^{2-}]$)) in solution. The AR and DR terms depend on solution composition (e.g., $[Ca^{2+}]$, $[HCO_3^-]$, $[CO_3^{2-}]$) and parameter values (e.g., attachment/detachment frequencies, kink formation energy, edge work, and surface speciation) in accordance with the ion-by-ion calcite growth model of Wolthers et al. (2012). All parameters used to calculate AR and DR can be found in the Matlab script that accompanies this article.

The behavior of these equations is shown in Figures 2a and 2b against data that have been adjusted to 5°C (Supplement S1 in Supporting Information S1). The data are from experiments in which the DIC pool likely remained in equilibrium with water during calcite growth, and thus, KIEs can be ascribed to attachment/detachment of $CO_3^{2-}$ and $HCO_3^-$ to/from the mineral surface. The observed growth rate- and pH-dependences place constraints on the carbon and oxygen isotope KFFs attending the crystal growth reactions (Table 2). Note that the oxygen isotope KFFs used to make these curves differ from those reported in Watkins et al. (2014) because the new values were calculated using Beck et al. (2005) rather than Wang et al. (2013) for the equilibrium oxygen isotope compositions of $HCO_3^-$ and $CO_3^{2-}$.

### 3.2. $^{13}C$-$^{18}O$ Clumped Isotopes

The ion-by-ion expression for clumped isotopes has the same form as for carbon and oxygen isotopes (i.e., Equations 57 and 58) but written for the mass 63 isotopologue:

$$ {}^{63}R_{CaCO_3} = \frac{[Ca3866]}{[Ca2666]} = \frac{{}^{63}R^{eq}_{CaCO_3} \cdot AR}{\frac{{}^{63}R^{eq}_{CaCO_3}(AR-DR)}{(1-\chi)\cdot{}^{63}\alpha^{kin}_{k_{B_1}}\cdot{}^{63}R_{CO_3^{2-}} + \chi\cdot{}^{63}\alpha^{kin}_{k_{B_2}}\cdot{}^{63}R_{HCO_3^-}}} + DR. \quad (59) $$

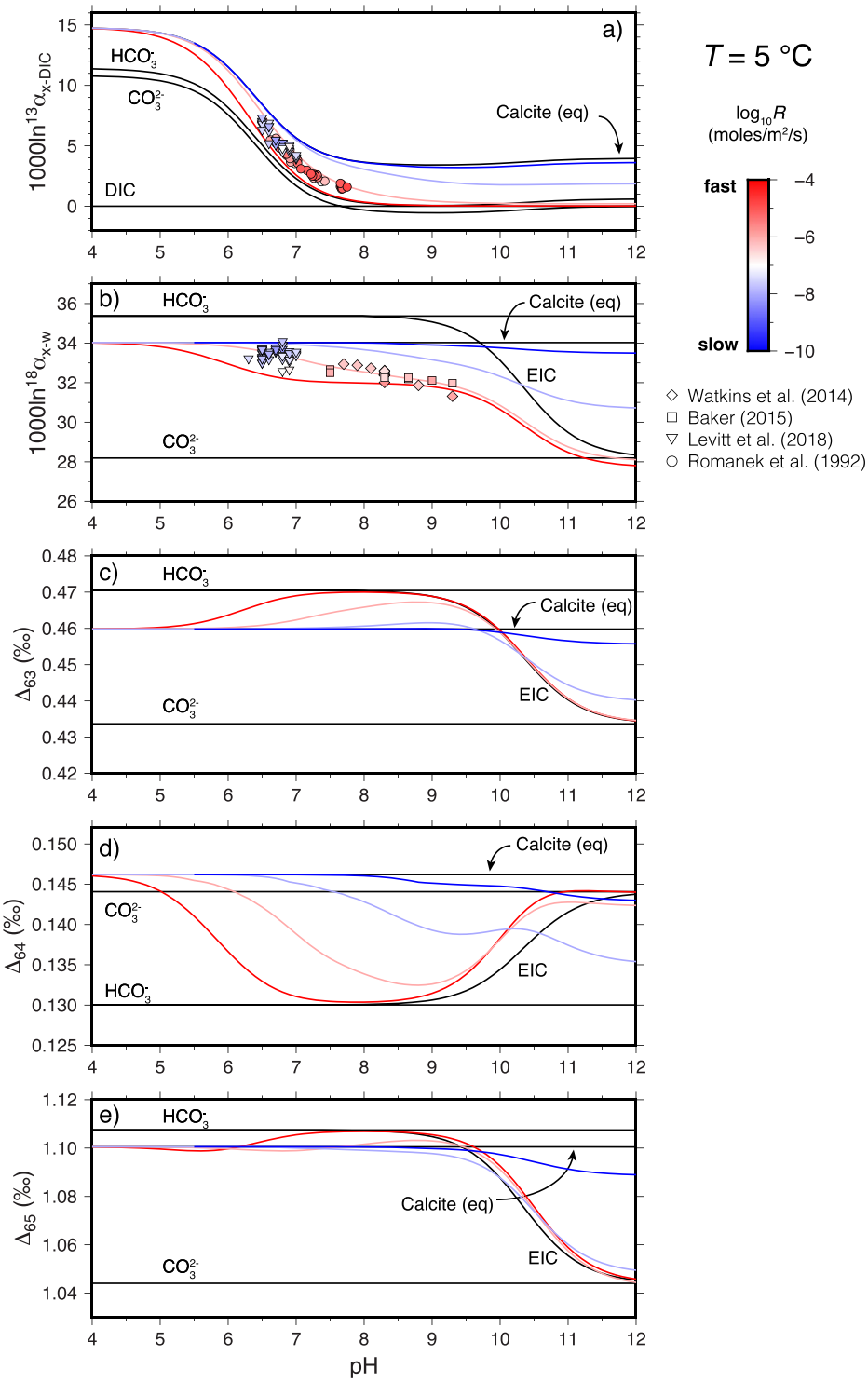


**Figure 2.** Behavior of the $CaCO_3$-DIC model at 5°C showing how the isotopic composition of calcite deviates from the equilibrated inorganic carbon pool (EIC = $HCO_3^-$, $CO_3^{2-}$) as a function of growth rate and pH. The data are from experiments in which the dissolved inorganic carbon pool likely remained in equilibrium with water during calcite growth, and thus, kinetic isotope effects can be ascribed to attachment/detachment of $CO_3^{2-}$ and $HCO_3^-$ to/from the mineral surface.

**Table 2**
*Equilibrium and Kinetic Fractionation Factors Used in the $CaCO_3$-$H_2O$ Model*

| Symbol | Value | Reference/Note |
|---|---|---|
| *Part I: Carbon isotope parameters* | | |
| $^{13}\alpha^{eq}_{CO_2-HCO_3^-}$ | $-9.866\,T_K^{-1} + 1.02412$ | Zhang et al. (1995) |
| $^{13}\alpha^{eq}_{CO_3^{2-}-HCO_3^-}$ | $-0.867\,T_K^{-1} + 1.00252$ | Zhang et al. (1995) |
| $^{13}\alpha^{eq}_{CaCO_3-HCO_3^-}$ | $\exp([1874.2\,T_K^{-1} - 3.3434]/1000)$ | Bottinga (1968); Zhang et al. (1995) |
| $^{13}\alpha^{kin}_{k_{B_1}}$ | 1.0000 | Watkins and Hunt (2015) |
| $^{13}\alpha^{kin}_{k_{B_2}}$ | 1.0000 | Watkins and Hunt (2015) |
| *Part II: Oxygen isotope parameters* | | |
| $^{18}\alpha^{eq}_{CO_2-H_2O}$ | $\exp(2520\,T_K^{-2} + 0.01212)$ | Beck et al. (2005) |
| $^{18}\alpha^{eq}_{HCO_3^--H_2O}$ | $\exp(2590\,T_K^{-2} + 0.00189)$ | Beck et al. (2005) |
| $^{18}\alpha^{eq}_{CO_3^{2-}-H_2O}$ | $\exp(2390\,T_K^{-2} - 0.00270)$ | Beck et al. (2005) |
| $^{18}\alpha^{eq}_{OH^--H_2O}$ | $5.6676 \times 10^{-5}\,T_K + 0.9622$ | based on Zeebe (2020) |
| $^{18}\alpha^{eq}_{CaCO_3-H_2O}$ | $\exp([17747\,T_K^{-1} - 29.777]/1000)$ | Watkins et al. (2014) |
| $^{18}\alpha^{kin}_{k_{B_1}}$ | 0.9995 | This study |
| $^{18}\alpha^{kin}_{k_{B_2}}$ | 0.9966 | This study |
| *Part III: $^{13}C$-$^{18}O$ clumped isotope parameters* | | |
| $\Delta^{eq}_{63,HCO_3^-}$ | $43655/T_K^2 - 23.643/T_K - 0.0088$ | Hill et al. (2020) |
| $\Delta^{eq}_{63,CO_3^{2-}}$ | $43187/T_K^2 + 34.833/T_K + 0.0007$ | Hill et al. (2020) |
| $\Delta^{eq}_{63,CaCO_3}$ | $43159/T_K^2 - 25.095/T_K - 0.0078$ | Hill et al. (2020) |
| $^{63}\alpha^{kin}_{k_{B_1}}$ | $^{13}\alpha^{kin}_{k_{B_1}} \cdot {}^{18}\alpha^{kin}_{k_{B_1}} + \epsilon_{k_{B_1}}$ | Watkins and Hunt (2015) |
| $^{63}\alpha^{kin}_{k_{B_2}}$ | $^{13}\alpha^{kin}_{k_{B_2}} \cdot {}^{18}\alpha^{kin}_{k_{B_2}} + \epsilon_{k_{B_2}}$. | Watkins and Hunt (2015) |
| *Part IV: $^{18}O$-$^{18}O$ clumped isotope parameters* | | |
| $\Delta^{eq}_{64,HCO_3^-}$ | $21842/T_K^2 - 50.457/T_K + 0.0291$ | Hill et al. (2020) |
| $\Delta^{eq}_{64,CO_3^{2-}}$ | $23492/T_K^2 - 52.842/T_K + 0.0304$ | Hill et al. (2020) |
| $\Delta^{eq}_{64,CaCO_3}$ | $23566/T_K^2 - 52.319/T_K + 0.0297$ | Hill et al. (2020) |
| $^{64}\alpha^{kin}_{k_{B_1}}$ | $^{18}\alpha^{kin}_{k_{B_1}} \cdot {}^{18}\alpha^{kin}_{k_{B_1}} + \epsilon'_{k_{B_1}}$, | This study |
| $^{64}\alpha^{kin}_{k_{B_2}}$ | $^{18}\alpha^{kin}_{k_{B_2}} \cdot {}^{18}\alpha^{kin}_{k_{B_2}} + \epsilon'_{k_{B_2}}$. | This study |
| *Part V: $^{13}C$-$^{18}O$-$^{18}O$ clumped isotope parameters* | | |
| $\Delta^{eq}_{65,HCO_3^-}$ | $112026/T_K^2 - 97.208/T_K + 0.009$ | Hill et al. (2020) |
| $\Delta^{eq}_{65,CO_3^{2-}}$ | $112667/T_K^2 - 123.11/T_K + 0.0304$ | Hill et al. (2020) |
| $\Delta^{eq}_{65,CaCO_3}$ | $112667/T_K^2 - 102.28/T_K + 0.012$ | Hill et al. (2020) |
| $^{65}\alpha^{kin}_{k_{B_1}}$ | $^{13}\alpha^{kin}_{k_{B_1}} \cdot {}^{18}\alpha^{kin}_{k_{B_1}} \cdot {}^{18}\alpha^{kin}_{k_{B_1}} + \epsilon''_{k_{B_1}}$, | This study |
| $^{65}\alpha^{kin}_{k_{B_2}}$ | $^{13}\alpha^{kin}_{k_{B_2}} \cdot {}^{18}\alpha^{kin}_{k_{B_2}} \cdot {}^{18}\alpha^{kin}_{k_{B_2}} + \epsilon''_{k_{B_2}}$. | This study |

Here, the values of ${}^{63}R_{CO_3^{2-}}$, ${}^{63}R_{HCO_3^-}$, and ${}^{63}R^{eq}_{CaCO_3}$ depend on the carbon and oxygen isotope composition of the crystal through the stochastic terms in:

$$ {}^{63}R_{CO_3^{2-}} = {}^{63}R^{*}_{CO_3^{2-}} \left( \frac{\Delta_{63,CO_3^{2-}}}{1000} + 1 \right), \tag{60} $$

$$ {}^{63}R_{HCO_3^-} = {}^{63}R^{*}_{HCO_3^-} \left( \frac{\Delta_{63,HCO_3^-}}{1000} + 1 \right), \tag{61} $$

and

$$ {}^{63}R^{eq}_{CaCO_3} = {}^{63}R^{eq*}_{CaCO_3} \left( \frac{\Delta^{eq}_{63,CaCO_3}}{1000} + 1 \right), \tag{62} $$

where

$$ {}^{63}R^{*}_{CO_3^{2-}} = 3 \cdot {}^{18}r_{CO_3^{2-}} \cdot {}^{13}r_{CO_3^{2-}}, \tag{63} $$

$$ {}^{63}R^{*}_{HCO_3^-} = 3 \cdot {}^{18}r_{CO_3^{2-}} \cdot {}^{13}r_{CO_3^{2-}} \cdot {}^{18}\alpha_{HCO_3^- - CO_3^{2-}} \cdot {}^{13}\alpha_{HCO_3^- - CO_3^{2-}}, \tag{64} $$

and

$$ {}^{63}R^{eq*}_{CaCO_3} = 3 \cdot {}^{18}r_{CO_3^{2-}} \cdot {}^{13}r_{CO_3^{2-}} \cdot {}^{18}\alpha^{eq}_{CaCO_3 - CO_3^{2-}} \, {}^{13}\alpha^{eq}_{CaCO_3 - CO_3^{2-}}. \tag{65} $$

The stochastic ratio for *nonequilibrium* calcite is given by:

$$ {}^{63}R^{*}_{CaCO_3} = 3 \cdot {}^{13}r_{CO_3^{2-}} \cdot {}^{18}r_{CO_3^{2-}} \cdot {}^{13}\alpha_{CaCO_3 - CO_3^{2-}} \cdot {}^{18}\alpha_{CaCO_3 - CO_3^{2-}}. \tag{66} $$

Combining these relationships and simplifying ultimately leads to:

$$ \frac{{}^{63}R_{CaCO_3}}{{}^{63}R^{*}_{CaCO_3}} = \frac{[\text{carbon isotopes}] \cdot [\text{oxygen isotopes}] \cdot \left( \frac{\Delta^{eq}_{63,CaCO_3}}{1000} + 1 \right)}{\text{AR} \left( \text{DR} + \frac{A \cdot \left( \frac{\Delta^{eq}_{63,CaCO_3}}{1000} + 1 \right) (\text{AR} - \text{DR})}{(1-\chi) \cdot {}^{63}\alpha^{kin}_{k_{B_1}} \left( \frac{\Delta_{63,CO_3^{2-}}}{1000} + 1 \right) + \chi \cdot {}^{63}\alpha^{kin}_{k_{B_2}} \cdot B \cdot \left( \frac{\Delta_{63,HCO_3^-}}{1000} + 1 \right)} \right)}, \tag{67} $$

where

$$ [\text{carbon isotopes}] = \left( \frac{{}^{13}\alpha^{eq}_{CaCO_3 - CO_3^{2-}} (\text{AR} - \text{DR})}{(1-\chi) \cdot {}^{13}\alpha^{kin}_{k_{B_1}} + \chi \cdot {}^{13}\alpha^{kin}_{k_{B_2}} \cdot {}^{13}\alpha_{HCO_3^- - CO_3^{2-}}} + \text{DR} \right), \tag{68} $$

$$ [\text{oxygen isotopes}] = \left( \frac{{}^{18}\alpha^{eq}_{CaCO_3 - CO_3^{2-}} (\text{AR} - \text{DR})}{(1-\chi) \cdot {}^{18}\alpha^{kin}_{k_{B_1}} + \chi \cdot {}^{18}\alpha^{kin}_{k_{B_2}} \cdot {}^{18}\alpha_{HCO_3^- - CO_3^{2-}}} + \text{DR} \right), \tag{69} $$

$$ A = {}^{13}\alpha^{eq}_{CaCO_3 - CO_3^{2-}} \cdot {}^{18}\alpha^{eq}_{CaCO_3 - CO_3^{2-}}, \tag{70} $$

$$ B = {}^{13}\alpha_{HCO_3^- - CO_3^{2-}} \cdot {}^{18}\alpha_{HCO_3^- - CO_3^{2-}}, \tag{71} $$

$$ {}^{63}\alpha^{kin}_{k_{B_1}} = {}^{13}\alpha^{kin}_{k_{B_1}} \cdot {}^{18}\alpha^{kin}_{k_{B_1}} + \epsilon_{k_{B_1}}, \tag{72} $$

and

$$^{63}\alpha^{\text{kin}}_{k_{B_2}} = {}^{13}\alpha^{\text{kin}}_{k_{B_2}} \cdot {}^{18}\alpha^{\text{kin}}_{k_{B_2}} + \epsilon_{k_{B_2}}. \tag{73}$$

This set of expressions is identical to Equation 38 of Watkins and Hunt (2015) but with some changes in notation and without the specification that DIC species are isotopically equilibrated with water. The $\epsilon_{k_{B_1}}$ and $\epsilon_{k_{B_2}}$ parameters are expected to be small, on the order of $10^{-5}$ (Watkins & Hunt, 2015).

The behavior of these equations is shown in Figure 2c using values of $\epsilon_{k_{B_1}} = \epsilon_{k_{B_2}} = 0$. For clarity, no data are shown in Figure 2c because different calibrations of the clumped isotope thermometer span a range of ~0.05‰ at a given temperature, with no resolvable dependence on pH (e.g., Kelson et al., 2017; Levitt et al., 2018). This range is greater than the range of model values depicted, implying that crystal growth-related kinetic effects are small for $\Delta_{63}$. As noted by Watkins and Hunt (2015), the $\Delta_{63}$ of calcite is indistinguishable from that of EIC at fast growth rates, implying that calcite can directly "inherit" the isotopic composition of EIC. Interestingly, this behavior in the fast growth limit does not hold for $^{18}$O-$^{18}$O and $^{13}$C-$^{18}$O-$^{18}$O clumped isotopes.

### 3.3. $^{18}$O-$^{18}$O Clumped Isotopes

The derivation for $^{18}$O-$^{18}$O clumped isotopes in calcite follows the same procedure (Supplement S2 in Supporting Information S1) and leads to an expression that is very similar to Equation 67 but does not depend on the carbon isotope composition of the crystal:

$$\frac{^{64}R_{CaCO_3}}{^{64}R^{*}_{CaCO_3}} = \frac{[\text{oxygen isotopes}] \cdot [\text{oxygen isotopes}] \cdot \left(\frac{\Delta^{\text{eq}}_{64,CaCO_3}}{1000} + 1\right)}{\text{AR}\left(\text{DR} + \frac{A' \cdot \left(\frac{\Delta^{\text{eq}}_{64,CaCO_3}}{1000} + 1\right)(\text{AR} - \text{DR})}{(1-\chi)\cdot {}^{64}\alpha^{\text{kin}}_{k_{B_1}}\left(\frac{\Delta_{64,CO_3^{2-}}}{1000} + 1\right) + \chi \cdot {}^{64}\alpha^{\text{kin}}_{k_{B_2}} \cdot B' \cdot \left(\frac{\Delta_{64,HCO_3^-}}{1000} + 1\right)}\right)}, \tag{74}$$

where

$$A' = {}^{18}\alpha^{\text{eq}}_{CaCO_3-CO_3^{2-}} \cdot {}^{18}\alpha^{\text{eq}}_{CaCO_3-CO_3^{2-}}, \tag{75}$$

$$B' = {}^{18}\alpha_{HCO_3^--CO_3^{2-}} \cdot {}^{18}\alpha_{HCO_3^--CO_3^{2-}}, \tag{76}$$

$$^{64}\alpha^{\text{kin}}_{k_{B_1}} = {}^{18}\alpha^{\text{kin}}_{k_{B_1}} \cdot {}^{18}\alpha^{\text{kin}}_{k_{B_1}} + \epsilon'_{k_{B_1}}, \tag{77}$$

and

$$^{64}\alpha^{\text{kin}}_{k_{B_2}} = {}^{18}\alpha^{\text{kin}}_{k_{B_2}} \cdot {}^{18}\alpha^{\text{kin}}_{k_{B_2}} + \epsilon'_{k_{B_2}}. \tag{78}$$

The behavior of these equations is shown in Figure 2d using values of $\epsilon'_{k_{B_1}} = \epsilon'_{k_{B_2}} = 0$. Unlike the case for $\Delta_{63}$, there is an offset in the $\Delta_{64}$ between calcite and EIC at fast growth rates. This difference in behavior is a manifestation of differences in the KFFs for carbon and oxygen isotopes. The nonequilibrium $\Delta_{63}$ of calcite is sensitive to the carbon isotope KFFs (see Section 4.3.1 of Uchikawa et al., 2021 for an explanation), which are equal to unity for the crystal growth reactions (Table 2; Watkins & Hunt, 2015). By contrast, the $\Delta_{64}$ of calcite is sensitive to the oxygen isotope KFFs, which are less than unity by some 2–4‰ (Table 2; Watkins et al., 2014), giving rise to a $\Delta_{64}$ of calcite that deviates from that of EIC at fast growth rates.

### 3.4. $^{13}$C-$^{18}$O-$^{18}$O Clumped Isotopes

The derivation for $^{13}$C-$^{18}$O-$^{18}$O clumped isotopes in calcite follows the same procedure (Supplement S3 in Supporting Information S1) and leads to the following expression:

$$\frac{{}^{65}R_{CaCO_3}}{{}^{65}R^{*}_{CaCO_3}} = \frac{[\text{carbon isotopes}]\cdot[\text{oxygen isotopes}]\cdot[\text{oxygen isotopes}]\cdot\left(\frac{\Delta^{eq}_{65,CaCO_3}}{1000}+1\right)}{AR^2\left(DR+\frac{A''\cdot\left(\frac{\Delta^{eq}_{65,CaCO_3}}{1000}+1\right)(AR-DR)}{(1-\chi)\cdot{}^{65}\alpha^{kin}_{k_{B_1}}\left(\frac{\Delta_{65,CO_3^{2-}}}{1000}+1\right)+\chi\cdot{}^{65}\alpha^{kin}_{k_{B_2}}\cdot B''\cdot\left(\frac{\Delta_{65,HCO_3^-}}{1000}+1\right)}\right)}, \tag{79}$$

where

$$A'' = {}^{13}\alpha^{eq}_{CaCO_3-CO_3^{2-}}\cdot{}^{18}\alpha^{eq}_{CaCO_3-CO_3^{2-}}\cdot{}^{18}\alpha^{eq}_{CaCO_3-CO_3^{2-}}, \tag{80}$$

$$B'' = {}^{13}\alpha_{HCO_3^--CO_3^{2-}}\cdot{}^{18}\alpha_{HCO_3^--CO_3^{2-}}\cdot{}^{18}\alpha_{HCO_3^--CO_3^{2-}}, \tag{81}$$

$${}^{65}\alpha^{kin}_{k_{B_1}} = {}^{13}\alpha^{kin}_{k_{B_1}}\cdot{}^{18}\alpha^{kin}_{k_{B_1}}\cdot{}^{18}\alpha^{kin}_{k_{B_1}}+\epsilon''_{k_{B_1}}, \tag{82}$$

and

$${}^{65}\alpha^{kin}_{k_{B_2}} = {}^{13}\alpha^{kin}_{k_{B_2}}\cdot{}^{18}\alpha^{kin}_{k_{B_2}}\cdot{}^{18}\alpha^{kin}_{k_{B_2}}+\epsilon''_{k_{B_2}}. \tag{83}$$

The behavior of these equations is shown in Figure 2e using values of $\epsilon''_{k_{B_1}} = \epsilon''_{k_{B_2}} = 0$. Since the $\Delta_{65}$ of calcite is sensitive to both carbon and oxygen isotope KFFs, the $\Delta_{65}$ of calcite is offset from that of EIC at fast growth rates, but the offset is less than that for $\Delta_{64}$ because the product of the carbon and oxygen isotope KFFs $\left({}^{13}\alpha^{kin}_{CaCO_3-EIC}\cdot{}^{18}\alpha^{kin}_{CaCO_3-EIC}\right)$ is closer to unity than the square of the oxygen isotope KFF $\left({}^{18}\alpha^{kin}_{CaCO_3-EIC}\cdot{}^{18}\alpha^{kin}_{CaCO_3-EIC}\right)$.

### 3.5. Summary of the $CaCO_3$-DIC Model

The $CaCO_3$-DIC model is a process-based model that can explain/predict the pH- and growth rate-dependence to the isotopic composition of calcite relative to EIC. The available data suggest that the KIEs for $\Delta_{63}$, $\Delta_{64}$, and $\Delta_{65}$ are too small to be resolved from the equilibrium calcite composition, given the current experimental reproducibility (Kelson et al., 2017; Levitt et al., 2018). It is nevertheless important to include the effects of $CaCO_3$ precipitation in models of clumped isotope KIEs for at least three reasons: (a) the rate of $CaCO_3$ growth affects the reversibility of hydration/hydroxylation reactions and their net KIEs, (b) small fractionations can lead to large KIEs due to isotopic distillation (Rayleigh fractionation) of the EIC pool, and (c) the fractionations are large enough to matter for carbon and oxygen isotopes and it would be inconsistent to treat clumped isotopes differently.

## 4. DIC-$H_2O$ Model

### 4.1. Carbon and Oxygen Isotopes (After Chen et al., 2018)

We begin this section by deriving the DIC-$H_2O$ model for carbon and oxygen isotopes of Chen et al. (2018). This is a necessary step for extending the model to $^{18}O$-$^{18}O$ and $^{13}C$-$^{18}O$-$^{18}O$ and clarifying some underlying assumptions. Along the way, we validate the model against analytical expressions available in the literature. Before we begin, note that the d[$C^{18}OO$]/dt notation of Chen et al. (2018) refers to the change in concentration of ([286] + [268]) as opposed to (a) a single permutation or (b) the total $^{18}O$ of $CO_2$, which would include [288].

#### 4.1.1. Isotope Reactions

For carbon and oxygen isotope calculations, we have the following exchange reactions:

$$266 + H_26 \underset{k_{-1}}{\overset{k_{+1}}{\rightleftharpoons}} H2666 + H \tag{84}$$

$$266 + 6H \underset{k_{-4}}{\overset{k_{+4}}{\rightleftharpoons}} H2666 \tag{85}$$

$$366 + H_26 \underset{c_{-1}}{\overset{c_{+1}}{\rightleftharpoons}} H3666 + H \tag{86}$$

$$366 + 6H \underset{c_{-4}}{\overset{c_{+4}}{\rightleftharpoons}} H3666 \tag{87}$$

$$266 + H_28 \underset{\frac{1}{3}a_{-1}}{\overset{a_{+1}}{\rightleftharpoons}} H2866 + H \tag{88}$$

$$286 + H_26 \underset{\frac{2}{3}b_{-1}}{\overset{b_{+1}}{\rightleftharpoons}} H2866 + H \tag{89}$$

$$266 + 8H \underset{\frac{1}{3}a_{-4}}{\overset{a_{+4}}{\rightleftharpoons}} H2866 \tag{90}$$

$$286 + 6H \underset{\frac{2}{3}b_{-4}}{\overset{b_{+4}}{\rightleftharpoons}} H2866 \tag{91}$$

For the reactions involving oxygen isotopes, the 1/3 and 2/3 factors are necessary for isotopic mass balance (Christensen et al., 2021; Uchikawa et al., 2021). Consider, for example, the two dehydration reactions involving H2866 (reactions 88 and 89). The right-hand sides of these two reactions are identical, but for every mole of H2866 that undergoes dehydration, ~2/3 goes to 286 and ~1/3 goes to $H_28$. The transfer is approximate because $a_{-1}$ and $b_{-1}$ are not exactly equal.

#### 4.1.2. Ordinary Differential Equations (ODEs)

From the reactions in Section 4.1.1, the following ODEs can be written:

$$\frac{d[266]}{dt} = -k_{+1}[266] + k_{-1}[E2666]\chi[H] - k_{+4}[266][6H] + k_{-4}[E2666]\chi \tag{92}$$

$$\frac{d[E2666]}{dt} = k_{+1}[266] - k_{-1}[E2666]\chi[H] \; k_{+4}[266][6H] - k_{-4}[E2666]\chi \tag{93}$$

$$\frac{d[366]}{dt} = -c_{+1}[366] + c_{-1}[E3666]^{13}\chi[H] - c_{+4}[366][6H] + c_{-4}[E3666]^{13}\chi \tag{94}$$

$$\frac{d[E3666]}{dt} = c_{+1}[366] - c_{-1}[E3666]^{13}\chi[H] \; c_{+4}[366][6H] - c_{-4}[E3666]^{13}\chi \tag{95}$$

$$\frac{d[286]}{dt} = -b_{+1}[286] + \frac{2}{3}b_{-1}[E2866]^{18}\chi[H] - b_{+4}[286][6H] + \frac{2}{3}b_{-4}[E2866]^{18}\chi \tag{96}$$

$$\begin{aligned}\frac{d[E2866]}{dt} = {} & a_{+1}[266]r_w - \frac{1}{3}a_{-1}[E2866]^{18}\chi[H] \\ & + a_{+4}[266][8H] - \frac{1}{3}a_{-4}[E2866]^{18}\chi \\ & + b_{+1}[286] - \frac{2}{3}b_{-1}[E2866]^{18}\chi[H] \\ & + b_{+4}[286][6H] - \frac{2}{3}b_{-4}[E2866]^{18}\chi\end{aligned} \tag{97}$$

where $[EIC]\chi = [HCO_3^-]$. The first two ODEs (Equations 92 and 93) describe chemical equilibration without contributions from less abundant isotopologues for reasons discussed in Supplement S4 in Supporting Information S1.

#### 4.1.3. $HCO_3^-$ Fraction of the EIC

As in the ion-by-ion model (Section 3.1), the $\chi$ terms represent the fraction of EIC that is $HCO_3^-$:

$$\chi = \frac{[\mathrm{H2666}]}{[\mathrm{H2666}] + [2666]} = \frac{1}{1 + \frac{K_2}{[\mathrm{H^+}]}}, \tag{98}$$

$$^{13}\chi = \frac{[\mathrm{H3666}]}{[\mathrm{H3666}] + [3666]} = \frac{1}{1 + \frac{K_2 \cdot {}^{13}\alpha^{\mathrm{eq}}_{CO_3^{2-}-HCO_3^-}}{[\mathrm{H^+}]}}, \tag{99}$$

and

$$^{18}\chi = \frac{[\mathrm{H2866}]}{[\mathrm{H2866}] + [2866]} = \frac{1}{1 + \frac{K_2 \cdot {}^{18}\alpha^{\mathrm{eq}}_{CO_3^{2-}-HCO_3^-}}{[\mathrm{H^+}]}}, \tag{100}$$

where $\alpha^{\mathrm{eq}}_{CO_3^{2-}-HCO_3^-}$ is the equilibrium fractionation factor between $CO_3^{2-}$ and $HCO_3^-$. These expressions are built upon the assumption of instantaneous $HCO_3^-$-$CO_3^{2-}$ and $H_2O$-$OH^-$ equilibration. This is a valid approximation because the equilibration time is on the order of $10^{-7}$ s, many orders of magnitude faster than the $CO_2$ hydration, hydroxylation, and crystal growth reactions (Zeebe & Wolf-Gladrow, 2001). For most practical applications, it is also appropriate to treat $[H_26]$ and $[H_28]$ as constant, implying there is an infinite reservoir of $H_2O$.

#### 4.1.4. Rate Constants and Fractionation Factors

The forward rate constants are directly related to KFFs. For the hydration reactions, we have

$$\frac{c_{+1}}{k_{+1}} = {}^{13}\alpha^{\mathrm{kin}}_{c_{+1}}, \tag{101}$$

$$\frac{a_{+1}}{k_{+1}} = {}^{18}\alpha^{\mathrm{kin}}_{a_{+1}}, \tag{102}$$

and

$$\frac{b_{+1}}{k_{+1}} = {}^{18}\alpha^{\mathrm{kin}}_{b_{+1}}. \tag{103}$$

For the hydroxylation reactions, we have

$$\frac{c_{+4}}{k_{+4}} = {}^{13}\alpha^{\mathrm{kin}}_{c_{+4}}, \tag{104}$$

$$\frac{a_{+4}}{k_{+4}} = {}^{18}\alpha^{\mathrm{kin}}_{a_{+4}}, \tag{105}$$

and

$$\frac{b_{+4}}{k_{+4}} = {}^{18}\alpha^{\mathrm{kin}}_{b_{+4}}. \tag{106}$$

The backward rate constants can be calculated from equilibrium constraints; that is:

$$k_{+1}[266]\,[H_26] = k_{-1}[\mathrm{H2666}][\mathrm{H}], \tag{107}$$

$$c_{+1}[366]\,[H_26] = c_{-1}[\mathrm{H3666}][\mathrm{H}], \tag{108}$$

$$a_{+1}[266]\,[H_28] = \frac{1}{3}a_{-1}[\mathrm{H2866}][\mathrm{H}], \tag{109}$$

$$b_{+1}[286]\,[H_26] = \frac{2}{3}b_{-1}[H2866][H], \tag{110}$$

$$k_{+4}[266][6H] = k_{-4}[H2666], \tag{111}$$

$$c_{+4}[366][6H] = c_{-4}[H3666], \tag{112}$$

$$a_{+4}[266][8H] = \frac{1}{3}a_{-4}[H2866], \tag{113}$$

and

$$b_{+4}[286][6H] = \frac{2}{3}b_{-4}[H2866]. \tag{114}$$

Converting isotopologue ratios to isotope ratios (Section 2.2) and rearranging yields the following relationships between rate constants and equilibrium constants:

$$\frac{k_{+1}}{k_{-1}} = \frac{[H2666][H]}{[266]\,[H_26]} = K_1, \tag{115}$$

$$\frac{c_{+1}}{c_{-1}} = \frac{{}^{13}r^{eq}_{HCO_3^-}[H2666][H]}{{}^{13}r^{eq}_{CO_2}[266]\,[H_26]} = K_1 \cdot {}^{13}\alpha^{eq}_{HCO_3^- - CO_2}, \tag{116}$$

$$\frac{a_{+1}}{a_{-1}} = \frac{(3)^{18}r^{eq}_{HCO_3^-}[H2666][H]}{(3)[266]\,[H_26]\,r_w} = K_1 \cdot {}^{18}\alpha^{eq}_{HCO_3^- - H_2O}, \tag{117}$$

$$\frac{b_{+1}}{b_{-1}} = \frac{(2\cdot 3)^{18}r^{eq}_{HCO_3^-}[H2666][H]}{(3\cdot 2)^{18}r^{eq}_{CO_2}[266]\,[H_26]} = K_1 \cdot {}^{18}\alpha^{eq}_{HCO_3^- - CO_2}, \tag{118}$$

$$\frac{k_{+4}}{k_{-4}} = \frac{[H2666]}{[266][6H]} = \frac{K_1}{K_w}, \tag{119}$$

$$\frac{c_{+4}}{c_{-4}} = \frac{{}^{13}r^{eq}_{HCO_3^-}[H2666]}{{}^{13}r^{eq}_{CO_2}[266][6H]} = \frac{K_1}{K_w} \cdot {}^{13}\alpha^{eq}_{HCO_3^- - CO_2}, \tag{120}$$

$$\frac{a_{+4}}{a_{-4}} = \frac{(3)^{18}r^{eq}_{HCO_3^-}[H2666]}{(3)^{18}r^{eq}_{OH^-}[266][6H]} = \frac{K_1}{K_w} \cdot \frac{{}^{18}\alpha^{eq}_{HCO_3^- - H_2O}}{{}^{18}\alpha^{eq}_{OH^- - H_2O}} \tag{121}$$

and

$$\frac{b_{+4}}{b_{-4}} = \frac{(2\cdot 3)^{18}r^{eq}_{HCO_3^-}[H2666]}{(3\cdot 2)^{18}r^{eq}_{CO_2}[266][6H]} = \frac{K_1}{K_w} \cdot {}^{18}\alpha^{eq}_{HCO_3^- - CO_2}. \tag{122}$$

In these equations, the equilibrium isotope ratios have been defined using only the singly substituted isotopologue. This is consistent with how we define oxygen isotope ratios and effectively removes the small errors, of order $10^{-6}$ (Guo & Zhou, 2019b) associated with the difference between Equations 12 and 14; that is, the small errors on ${}^{18}r$ values associated with non-stochasticity.

An up-to-date compilation of rate constants, equilibrium constants, and isotopic fractionation factors is provided in Table 3. Outputs from numerical integration of the coupled set of ODEs (Equations 92–97) are compared to analytical expressions in Supplement S5 in Supporting Information S1.

### 4.2. $^{13}C$-$^{18}O$ Clumped Isotopes (After Uchikawa et al., 2021)

The above framework was extended to $^{13}C$-$^{18}O$ clumped isotopes by Uchikawa et al. (2021), and much of what follows has also been presented previously. Here, an abbreviated re-derivation is provided that explicitly tracks

**Table 3**
*Parameters for $^{13}C/^{12}C$ and $^{18}O/^{16}O$ Ratios*

| Symbol | Expression | Reference/Note |
|---|---|---|
| *Part I: Chemical parameters* | | |
| $K_1$ | $\frac{[H2666][H]}{[266][H_26]}$, $[H_26] = 1$ | Millero et al. (2007) |
| $K_2$ | $\frac{[2666][H]}{[H2666]}$ | Millero et al. (2007) |
| $K_w$ | [6H][H] | DOE (1994) |
| $k_{+1}$ | $\log_{10}k_{+1} = 329.85 - 110.541\log_{10}(T_K) - \frac{17265.4}{T_K}$ | Uchikawa and Zeebe (2012) |
| $k_{-1}$ | $k_{-1} = k_{+1}/K_1$ | – |
| $k_{+4}$ | $\log_{10}k_{+4} = 13.635 - \frac{2895}{T_K}$ | Uchikawa and Zeebe (2012) |
| $k_{-4}$ | $k_{-4} = k_{+4}\frac{K_w}{K_1}$ | – |
| $\chi$ | $\chi = \frac{1}{1+\frac{K_2}{[H^+]}}$ | – |
| *Part II: Carbon isotope parameters* | | |
| $^{13}\alpha^{kin}_{c_{+1}}$ | 0.9872 | Yumol et al. (2020) |
| $^{13}\alpha^{kin}_{c_{+4}}$ | 0.9814 | Christensen et al. (2021) |
| $c_{+1}$ | $c_{+1} = {}^{13}\alpha^{kin}_{c_{+1}} \cdot k_{+1}$ | – |
| $c_{-1}$ | $c_{-1} = c_{+1}/\left(K_1 \cdot {}^{13}\alpha^{eq}_{HCO_3^- - CO_2}\right)$ | – |
| $c_{+4}$ | $c_{+4} = {}^{13}\alpha^{kin}_{c_{+4}} \cdot k_{+4}$ | – |
| $c_{-4}$ | $c_{-4} = c_{+4}/\left(\frac{K_1}{K_w} \cdot {}^{13}\alpha^{eq}_{HCO_3^- - CO_2}\right)$ | – |
| $^{13}\chi$ | $^{13}\chi = \frac{1}{1+\frac{1}{K_2 \cdot {}^{13}\alpha^{eq}_{CO_3^{2-} - HCO_3^-}}}$ | – |
| *Part III: Oxygen isotope parameters* | | |
| $^{18}\alpha^{kin}_{a_{+1}}$ | 1.0000 | Yumol et al. (2020) |
| $^{18}\alpha^{kin}_{b_{+1}}$ | 0.9812 | Yumol et al. (2020) |
| $^{18}\alpha^{kin}_{a_{+4}}$ | 0.9706[a] | Christensen et al. (2021)[a] |
| $^{18}\alpha^{kin}_{b_{+4}}$ | 1.0000 | Christensen et al. (2021) |
| $a_{+1}$, $b_{+1}$ | $a_{+1} = {}^{18}\alpha^{kin}_{a_{+1}} \cdot k_{+1}$ | – |
| | $b_{+1} = {}^{18}\alpha^{kin}_{b_{+1}} \cdot k_{+1}$ | – |
| $a_{-1}$, $b_{-1}$ | $a_{-1} = a_{+1}/\left(K_1 \cdot {}^{18}\alpha_{HCO_3^- - H_2O}\right)$ | – |
| | $b_{-1} = b_{+1}/\left(K_1 \cdot {}^{18}\alpha_{HCO_3^- - CO_2}\right)$ | – |
| $a_{+4}$, $b_{+4}$ | $a_{+4} = {}^{18}\alpha^{kin}_{a_{+4}} \cdot k_{+4}$ | – |
| | $b_{+4} = {}^{18}\alpha^{kin}_{b_{+4}} \cdot k_{+4}$ | – |
| $a_{-4}$, $b_{-4}$ | $a_{-4} = a_{+4}/\left(\frac{K_1}{K_w}\frac{{}^{18}\alpha_{HCO_3^- - H_2O}}{{}^{18}\alpha_{OH^- - H_2O}}\right)$ | – |
| | $b_{-4} = b_{+4}/\left(\frac{K_1}{K_w}{}^{18}\alpha_{HCO_3^- - CO_2}\right)$ | – |
| $^{18}\chi$ | $^{18}\chi = \frac{1}{1+\frac{1}{K_2 \cdot {}^{18}\alpha^{eq}_{CO_3^{2-} - HCO_3^-}}}$ | – |

[a]Updated value that has been corrected for a conversion error in Christensen et al. (2021) betwen VPDB-$CO_2$, VPDB, and VSMOW scales.

the 1/3 and 2/3 factors for oxygen isotope bookkeeping and does not fold the acid fractionation factors into the expressions for EIC. Additionally, we clarify a difference in the final expressions for the rate constants that would otherwise lead to issues when extending the model to $^{18}O$-$^{18}O$ and $^{13}C$-$^{18}O$-$^{18}O$ clumped isotopes.

#### 4.2.1. Isotope Reactions

To add clumped isotopes to the model, we need to include the reactions involving $^{13}C$-$^{18}O$ "clumps" in $CO_2$ and $HCO_3^-$:

$$366 + H_28 \underset{\frac{1}{3}p_{-1}}{\overset{p_{+1}}{\rightleftharpoons}} H3866 + H \tag{123}$$

$$386 + H_26 \underset{\frac{2}{3}s_{-1}}{\overset{s_{+1}}{\rightleftharpoons}} H3866 + H \tag{124}$$

$$366 + 8H \underset{\frac{1}{3}p_{-4}}{\overset{p_{+4}}{\rightleftharpoons}} H3866 \tag{125}$$

$$386 + 6H \underset{\frac{2}{3}s_{-4}}{\overset{s_{+4}}{\rightleftharpoons}} H3866 \tag{126}$$

Rate constants for the clumped isotope reactions are denoted $p$ for "primary" and $s$ for "secondary" following Guo (2020). In the primary reactions, a clumped isotopologue is created from reactants that are singly substituted.

#### 4.2.2. ODEs

From the preceding reactions we obtain the following ODEs:

$$\begin{aligned}\frac{d[386]}{dt} = &-s_{+1}[386] + \frac{2}{3}s_{-1}[E3866]^{63}\chi[H] \\ &-s_{+4}[386][6H] + \frac{2}{3}s_{-4}[E3866]^{63}\chi\end{aligned} \tag{127}$$

and

$$\begin{aligned}\frac{d[E3866]}{dt} = &\ p_{+1}[366]r_w - \frac{1}{3}p_{-1}[E3866]^{63}\chi[H] \\ &+ p_{+4}[366][8H] - \frac{1}{3}p_{-4}[E3866]^{63}\chi \\ &+ s_{+1}[386] - \frac{2}{3}s_{-1}[E3866]^{63}\chi[H] \\ &+ s_{+4}[386][6H] - \frac{2}{3}s_{-4}[E3866]^{63}\chi.\end{aligned} \tag{128}$$

The next task is to derive the $^{63}\chi$ parameter as well as the rate constants.

#### 4.2.3. $HCO_3^-$ Fraction of the EIC

The $^{63}\chi$ term is analogous to $^{13}\chi$ and $^{18}\chi$ and is used to instantaneously redistribute the clumped isotopes between $HCO_3^-$ and $CO_3^{2-}$ so that these two species are in clumped isotopic equilibrium with each other. The expression takes the same form as the other $\chi$ terms because the fraction of clumped EIC that is in the form of $HCO_3^-$ has the same pH dependence as for standard isotope ratios (Hill et al., 2014):

$$^{63}\chi = \frac{1}{1 + \frac{^{63}K_2}{[H^+]}}, \tag{129}$$

where $^{63}K_2$ is the equilibrium constant for the deprotonation reaction:

$$^{63}K_2 = \frac{[3866][H]}{[H3866]}. \tag{130}$$

This can be expressed in terms of the equilibrium $\Delta_{63}$ values of $HCO_3^-$ and $CO_3^{2-}$. First, the top and bottom are multiplied by a common factor:

$$^{63}K = \frac{[3866][H]}{[H3866]} \cdot \frac{\frac{[H2666]}{[H3666][H2866]}}{\frac{[H2666]}{[H3666][H2866]}} \cdot \frac{\frac{[2666]}{[3666][2866]}}{\frac{[2666]}{[3666][2866]}} \cdot \frac{[2666]}{[2666]} \cdot \frac{[H2666]}{[H2666]}, \tag{131}$$

which upon rearrangement yields

$$^{63}K_2 = \frac{\frac{[3866][2666]}{[3666][2866]}}{\frac{[H3866][H2666]}{[H3666][H2866]}} \cdot \frac{\frac{[H2666]}{[H3666]}}{\frac{[2666]}{[3666]}} \cdot \frac{\frac{[H2666]}{[H2866]}}{\frac{[2666]}{[2866]}} \cdot \frac{[2666][H]}{[H2666]}. \tag{132}$$

Converting isotopologue ratios to isotope ratios leads to

$$^{63}K_2 = {}^{63}\alpha^{eq}_{CO_3^{2-}-HCO_3^-} \cdot {}^{13}\alpha^{eq}_{CO_3^{2-}-HCO_3^-} \cdot {}^{18}\alpha^{eq}_{CO_3^{2-}-HCO_3^-} \cdot K_2, \tag{133}$$

where

$${}^{63}\alpha^{eq}_{CO_3^{2-}-HCO_3^-} = \frac{\left(\frac{\Delta^{eq}_{63,CO_3^{2-}}}{1000} + 1\right)}{\left(\frac{\Delta^{eq}_{63,HCO_3^-}}{1000} + 1\right)}. \tag{134}$$

#### 4.2.4. Rate Constants and Fractionation Factors

Guo (2020) defined the "intrinsic KFF" for clumped isotopes relative to the product of the carbon and oxygen KFFs:

$$^{13-18}\mathrm{KIE}_{p_{+1}} = \frac{^{13-18}\alpha^{kin}_{p_{+1}}}{{}^{18}\alpha^{kin}_{a_{+1}} \cdot {}^{13}\alpha^{kin}_{c_{+1}}} = \frac{\frac{p_{+1}}{k_{+1}}}{\frac{c_{+1}}{k_{+1}}\frac{a_{+1}}{k_{+1}}}. \tag{135}$$

A $^{13-18}\mathrm{KIE}_{p_{+1}} = 1$ means the intrinsic KFF does not deviate from the product of the corresponding oxygen and carbon isotope KFFs. This is analogous to the case where $\epsilon_{k_{B_1}} = \epsilon_{k_{B_2}} = 0$ in the $CaCO_3$-DIC model (Section 3.2). Guo's theoretical values for the $^{13-18}$KIEs are provided in Table 4.

Rearranging Equation 135 leads to an expression for $p_{+1}$:

$$p_{+1} = \frac{^{13-18}\mathrm{KIE}_{p_{+1}} c_{+1} a_{+1}}{k_{+1}}, \tag{136}$$

where $^{13-18}\mathrm{KIE}_{p_{+1}}$ is treated as a known quantity (Guo, 2020). To obtain $p_{-1}$, we use the equilibrium constraint from the corresponding reaction:

$$\frac{p_{+1}}{p_{-1}} = \frac{\frac{1}{3}[H3866][H]}{[366]\,[H_28]}. \tag{137}$$

By multiplying the top and bottom by a common factor, we can write:

$$\frac{p_{+1}}{p_{-1}} = \frac{\frac{1}{3}[H3866][H]}{[366]\,[H_28]} \cdot \frac{\frac{[H2666]}{[H3666][H2866]}}{\frac{[H2666]}{[H3666][H2866]}} \cdot \frac{\frac{[H2666]}{[266]}}{\frac{[H2666]}{[266]}} \cdot \frac{\frac{1}{H_26}}{\frac{1}{H_26}}, \tag{138}$$

which upon rearrangement leads to

$$\frac{p_{+1}}{p_{-1}} = \frac{\frac{1}{3}[H3866][H2666]}{[H3666][H2866]} \cdot \frac{[H2666][H]}{[266][H26]} \cdot \frac{\frac{[H3666]}{[H2666]}}{\frac{[366]}{[266]}} \cdot \frac{\frac{[H2866]}{[H2666]}}{\frac{[H28]}{[H26]}}. \tag{139}$$

Converting isotopologue ratios to isotope ratios leads to

**Table 4**
*Parameters for $^{13}C$-$^{18}O$ Clumped Isotopes*

| Symbol | Value | Reference/Note |
|---|---|---|
| $\Delta^{eq}_{47,CO_2}$ | $26447/T_K^2 + 285.51/T_K - 0.3004$ | Wang et al. (2004) |
| $\Delta^{eq}_{63,HCO_3^-}$ | [see Table 2] | – |
| $\Delta^{eq}_{63,CO_3^{2-}}$ | [see Table 2] | – |
| $\left({}^{47}R/{}^{47}R^*\right)^{eq}_{CO_2}$ | $\Delta^{eq}_{47,CO_2}/1000 + 1$ | – |
| $\left({}^{63}R/{}^{63}R^*\right)^{eq}_{HCO_3^-}$ | $\Delta^{eq}_{63,HCO_3^-}/1000 + 1$ | – |
| $\left({}^{63}R/{}^{63}R^*\right)^{eq}_{CO_3^{2-}}$ | $\Delta^{eq}_{63,CO_3^{2-}}/1000 + 1$ | – |
| ${}^{63}\alpha^{eq}_{CO_3^{2-}-HCO_3^-}$ | $\left({}^{63}R/{}^{63}R^*\right)^{eq}_{CO_3^{2-}}/\left({}^{63}R/{}^{63}R^*\right)^{eq}_{HCO_3^-}$ | – |
| ${}^{63}K_2$ | ${}^{63}\alpha^{eq}_{CO_3^{2-}-HCO_3^-} \cdot {}^{13}\alpha^{eq}_{CO_3^{2-}-HCO_3^-} \cdot {}^{18}\alpha^{eq}_{CO_3^{2-}-HCO_3^-} \cdot K_2$ | – |
| ${}^{63}\chi$ | $\frac{1}{1+\frac{{}^{63}K_2}{[H^+]}}$ | – |
| ${}^{13-18}\mathrm{KIE}p_{+1}$ | $(4613.8393/T_K^2 - 4.0389/T_K - 0.185\ )/1000 + 1$ | Guo (2020) |
| ${}^{13-18}\mathrm{KIE}s_{+1}$ | $(-5705.688/T_K^2 - 41.5925/T_K - 0.015\ )/1000 + 1$ | Guo (2020) |
| ${}^{13-18}\mathrm{KIE}p_{+4}$ | $(-902.7635/T_K^2 + 157.1718/T_K - 0.533\ )/1000 + 1$ | Guo (2020) |
| ${}^{13-18}\mathrm{KIE}s_{+4}$ | $(-11771.2832/T_K^2 - 62.7060/T_K + 0.168\ )/1000 + 1$ | Guo (2020) |
| $p_{+1}$, $s_{+1}$ | $p_{+1} = \left({}^{13-18}\mathrm{KIE}p_{+1} \cdot c_{+1} \cdot a_{+1}\right)/k_{+1}$ | Uchikawa et al. (2021) |
| | $s_{+1} = \left({}^{13-18}\mathrm{KIE}s_{+1} \cdot c_{+1} \cdot b_{+1}\right)/k_{+1}$ | Uchikawa et al. (2021) |
| $p_{-1}$, $s_{-1}$ | $p_{-1} = p_{+1}/\left[\left({}^{63}R/{}^{63}R^*\right)^{eq}_{HCO_3^-} \cdot K_1 \cdot {}^{13}\alpha^{eq}_{HCO_3^- - CO_2} \cdot {}^{18}\alpha^{eq}_{HCO_3^- - H_2O}\right]$ | – |
| | $s_{-1} = s_{+1} \cdot \left[\left({}^{47}R/{}^{47}R^*\right)^{eq}_{CO_2}\right]/\left[\left({}^{63}R/{}^{63}R^*\right)^{eq}_{HCO_3^-} \cdot K_1 \cdot {}^{13}\alpha^{eq}_{HCO_3^- - CO_2} \cdot {}^{18}\alpha^{eq}_{HCO_3^- - CO_2}\right]$ | – |
| $p_{+4}$, $s_{+4}$ | $p_{+4} = \left({}^{13-18}\mathrm{KIE}p_{+4} \cdot c_{+4} \cdot a_{+4}\right)/k_{+4}$ | Uchikawa et al. (2021) |
| | $s_{+4} = \left({}^{13-18}\mathrm{KIE}s_{+4} \cdot c_{+4} \cdot b_{+4}\right)/k_{+4}$ | Uchikawa et al. (2021) |
| $p_{-4}$, $s_{-4}$ | $p_{-4} = p_{+4}/\left[\left({}^{63}R/{}^{63}R^*\right)^{eq}_{HCO_3^-} \cdot K_1/K_w \cdot {}^{13}\alpha^{eq}_{HCO_3^- - CO_2} \cdot {}^{18}\alpha^{eq}_{HCO_3^- - OH^-}\right]$ | – |
| | $s_{-4} = s_{+4} \cdot \left[\left({}^{47}R/{}^{47}R^*\right)^{eq}_{CO_2}\right]/\left[\left({}^{63}R/{}^{63}R^*\right)^{eq}_{HCO_3^-} \cdot K_1/K_w \cdot {}^{13}\alpha^{eq}_{HCO_3^- - CO_2} \cdot {}^{18}\alpha^{eq}_{HCO_3^- - CO_2}\right]$ | – |

$$\frac{p_{+1}}{p_{-1}} = \frac{1}{3} \cdot \left(\frac{{}^{63}R}{{}^{63}R^*}\right)^{eq}_{HCO_3^-} \cdot K_1 \cdot \frac{{}^{13}r^{eq}_{HCO_3^-}}{{}^{13}r^{eq}_{CO_2}} \cdot \frac{3 \cdot {}^{18}r^{eq}_{HCO_3^-}}{r_w}. \tag{140}$$

The factors of 3 and 1/3 cancel and we get:

$$\frac{p_{+1}}{p_{-1}} = \left(\frac{{}^{63}R}{{}^{63}R^*}\right)^{eq}_{HCO_3^-} \cdot K_1 \cdot {}^{13}\alpha^{eq}_{HCO_3^- - CO_2} \cdot {}^{18}\alpha^{eq}_{HCO_3^- - H_2O} \tag{141}$$

Similar expressions can be derived for the remaining clumped isotope rate constants (Supplement S6 in Supporting Information S1), ultimately leading to:

$$\frac{s_{+1}}{s_{-1}} = \frac{\left(\frac{{}^{63}R}{{}^{63}R^*}\right)^{eq}_{HCO_3^-} \cdot K_1 \cdot {}^{13}\alpha^{eq}_{HCO_3^- - CO_2} \cdot {}^{18}\alpha^{eq}_{HCO_3^- - CO_2}}{\left(\frac{{}^{47}R}{{}^{47}R^*}\right)^{eq}_{CO_2}}, \tag{142}$$

$$\frac{p_{+4}}{p_{-4}} = \left(\frac{{}^{63}R}{{}^{63}R^*}\right)^{eq}_{HCO_3^-} \cdot \frac{K_1}{K_w} \cdot {}^{13}\alpha^{eq}_{HCO_3^- - CO_2} \cdot {}^{18}\alpha^{eq}_{HCO_3^- - OH^-}, \tag{143}$$

and

$$\frac{S_{+4}}{S_{-4}} = \frac{\left(\frac{^{63}R}{^{63}R^*}\right)^{eq}_{HCO_3^-} \cdot \frac{K_1}{K_w} \cdot {}^{18}\alpha^{eq}_{HCO_3^- - CO_2} \cdot {}^{13}\alpha^{eq}_{HCO_3^- - CO_2}}{\left(\frac{^{47}R}{^{47}R^*}\right)^{eq}_{CO_2}} \tag{144}$$

These expressions for the rate constants are nearly identical to those of Uchikawa et al. (2021). The only significant difference is that they use ${}^{47}K^{eq}_{CO_2}$ and ${}^{63}K^{eq}_{HCO_3^-}$ instead of $\left({}^{47}R/{}^{47}R^*\right)^{eq}_{CO_2}$ and $\left({}^{63}R/{}^{63}R^*\right)^{eq}_{HCO_3^-}$, respectively. This works for $^{13}$C-$^{18}$O clumped isotopes because the quantities are equivalent, but breaks down for $^{18}$O-$^{18}$O and $^{13}$C-$^{18}$O-$^{18}$O clumped isotopes. A compilation of the parameters needed to solve the ODEs (Equations 127 and 128) is provided in Table 4.

### 4.3. $^{18}$O-$^{18}$O Clumped Isotopes

#### 4.3.1. Isotope Reactions

To add the mass 48 and 64 isotopologues to the model, we need to include the reactions involving $^{18}$O-$^{18}$O "clumps" in $CO_2$ and $HCO_3^-$:

$$286 + H_28 \underset{\frac{2}{3}p'_{-1}}{\overset{p'_{+1}}{\rightleftharpoons}} H2886 + H \tag{145}$$

$$288 + H_26 \underset{\frac{1}{3}s'_{-1}}{\overset{s'_{+1}}{\rightleftharpoons}} H2886 + H \tag{146}$$

$$286 + 8H \underset{\frac{2}{3}p'_{-4}}{\overset{p'_{+4}}{\rightleftharpoons}} H2886 \tag{147}$$

$$288 + 6H \underset{\frac{1}{3}s'_{-4}}{\overset{s'_{+4}}{\rightleftharpoons}} H2886 \tag{148}$$

Note that the primary reactions have a factor of 2/3 on the back reaction whereas for standard clumped isotope reactions, the primary reactions had a factor of 1/3.

#### 4.3.2. ODEs

From the preceding reactions we obtain the following ODEs:

$$\begin{aligned}\frac{d[288]}{dt} &= -s'_{+1}[288] + \frac{1}{3}s'_{-1}[E2886]^{64}\chi[H] \\ &\quad -s'_{+4}[288][6H] + \frac{1}{3}s'_{-4}[E2886]^{64}\chi\end{aligned} \tag{149}$$

$$\begin{aligned}\frac{d[E2886]}{dt} &= p'_{+1}[286]r_w - \frac{2}{3}p'_{-1}[E2886]^{64}\chi[H] \\ &\quad + p'_{+4}[286][8H] - \frac{2}{3}p'_{-4}[E2886]^{64}\chi \\ &\quad + s'_{+1}[288] - \frac{1}{3}s'_{-1}[E2886]^{64}\chi[H] \\ &\quad + s'_{+4}[288][6H] - \frac{1}{3}s'_{-4}[E2886]^{64}\chi\end{aligned} \tag{150}$$

#### 4.3.3. Fraction of $HCO_3^-$ in the EIC

The derivation of ${}^{64}\chi$ is provided in Supplement S7 in Supporting Information S1 with the resulting expression provided in Table 5.

#### 4.3.4. Rate Constants

The derivation of $p'$ and $s'$ rate constants is provided in Supplement S7 in Supporting Information S1 with results compiled in Table 5.

**Table 5**
*Parameters for $^{18}O$-$^{18}O$ Clumped Isotopes*

| Symbol | Value | Reference/Note |
|---|---|---|
| $\Delta^{eq}_{48,CO_2}$ | $29306/T_K^2 + 93.885/T_K - 0.2914$ | Wang et al. (2004) |
| $\Delta^{eq}_{64,HCO_3^-}$ | [see Table 2] | – |
| $\Delta^{eq}_{64,CO_3^{2-}}$ | [see Table 2] | – |
| $\left({}^{48}R/{}^{48}R^*\right)^{eq}_{CO_2}$ | $\Delta^{eq}_{48,CO_2}/1000 + 1$ | – |
| $\left({}^{64}R/{}^{64}R^*\right)^{eq}_{HCO_3^-}$ | $\Delta^{eq}_{64,HCO_3^-}/1000 + 1$ | – |
| $\left({}^{64}R/{}^{64}R^*\right)^{eq}_{CO_3^{2-}}$ | $\Delta^{eq}_{64,CO_3^{2-}}/1000 + 1$ | – |
| ${}^{64}\alpha^{eq}_{CO_3^{2-}-HCO_3^-}$ | $\left({}^{64}R/{}^{64}R^*\right)^{eq}_{CO_3^{2-}} / \left({}^{64}R/{}^{64}R^*\right)^{eq}_{HCO_3^-}$ | – |
| ${}^{64}K_2$ | ${}^{64}\alpha^{eq}_{CO_3^{2-}-HCO_3^-} \cdot {}^{18}\alpha^{eq}_{CO_3^{2-}-HCO_3^-} \cdot K_2$ | – |
| ${}^{64}\chi$ | $\frac{1}{1+\frac{{}^{64}K_2}{[H^+]}}$ | – |
| ${}^{18-18}\mathrm{KIE}_{p'_{+1}}$ | $(-13249.5324/T_K^2 - 37.8964/T_K + 0.027)/1000 + 1$ | Guo (2020) |
| ${}^{18-18}\mathrm{KIE}_{s'_{+1}}$ | $(-18411.4121/T_K^2 - 3.7575/T_K + 0.074)/1000 + 1$ | Guo (2020) |
| ${}^{18-18}\mathrm{KIE}_{p'_{+4}}$ | $(-5859.1625/T_K^2 - 3.7964/T_K - 0.197)/1000 + 1$ | Guo (2020) |
| ${}^{18-18}\mathrm{KIE}_{s'_{+4}}$ | $(-12333.8137/T_K^2 + 8.6005/T_K + 0.024)/1000 + 1$ | Guo (2020) |
| $p'_{+1}, s'_{+1}$ | $p'_{+1} = \left({}^{18-18}\mathrm{KIE}_{p'_{+1}} \cdot b_{+1} \cdot a_{+1}\right)/k_{+1}$ | – |
| | $s'_{+1} = \left({}^{18-18}\mathrm{KIE}_{s'_{+1}} \cdot b_{+1} \cdot b_{+1}\right)/k_{+1}$ | – |
| $p'_{-1}, s'_{-1}$ | $p'_{-1} = p'_{+1} / \left[\left({}^{64}R/{}^{64}R^*\right)^{eq}_{HCO_3^-} \cdot K_1 \cdot {}^{18}\alpha^{eq}_{HCO_3^--CO_2} \cdot {}^{18}\alpha^{eq}_{HCO_3^--H_2O}\right]$ | – |
| | $s'_{-1} = s'_{+1} \cdot \left[\left({}^{48}R/{}^{48}R^*\right)^{eq}_{CO_2}\right] / \left[\left({}^{64}R/{}^{64}R^*\right)^{eq}_{HCO_3^-} \cdot K_1 \cdot {}^{18}\alpha^{eq}_{HCO_3^--CO_2} \cdot {}^{18}\alpha^{eq}_{HCO_3^--CO_2}\right]$ | – |
| $p'_{+4}, s'_{+4}$ | $p'_{+4} = \left({}^{18-18}\mathrm{KIE}_{p'_{+4}} \cdot b_{+4} \cdot a_{+4}\right)/k_{+4}$ | – |
| | $s'_{+4} = \left({}^{18-18}\mathrm{KIE}_{s'_{+4}} \cdot b_{+4} \cdot b_{+4}\right)/k_{+4}$ | – |
| $p'_{-4}, s'_{-4}$ | $p'_{-4} = p'_{+4} / \left[\left({}^{64}R/{}^{64}R^*\right)^{eq}_{HCO_3^-} \cdot K_1/K_w \cdot {}^{18}\alpha^{eq}_{HCO_3^--CO_2} \cdot {}^{18}\alpha^{eq}_{HCO_3^--OH^-}\right]$ | – |
| | $s'_{-4} = s'_{+4} \cdot \left[\left({}^{48}R/{}^{48}R^*\right)^{eq}_{CO_2}\right] / \left[\left({}^{64}R/{}^{64}R^*\right)^{eq}_{HCO_3^-} \cdot K_1/K_w \cdot {}^{18}\alpha^{eq}_{HCO_3^--CO_2} \cdot {}^{18}\alpha^{eq}_{HCO_3^--CO_2}\right]$ | – |

### 4.4. $^{13}C$-$^{18}O$-$^{18}O$ Clumped Isotopes

#### 4.4.1. Isotope Reactions

To add the mass 49 and 65 isotopologues to the model, we need to include the reactions involving $^{13}O$-$^{18}O$-$^{18}O$ "clumps" in $CO_2$ and $HCO_3^-$:

$$386 + H_28 \underset{\frac{2}{3}p''_{-1}}{\overset{p''_{+1}}{\rightleftharpoons}} H3886 + H \tag{151}$$

$$388 + H_26 \underset{\frac{1}{3}s''_{-1}}{\overset{s''_{+1}}{\rightleftharpoons}} H3886 + H \tag{152}$$

$$386 + 8H \underset{\frac{2}{3}p''_{-4}}{\overset{p''_{+4}}{\rightleftharpoons}} H3886 \tag{153}$$

$$388 + 6H \underset{\frac{1}{3}s''_{-4}}{\overset{s''_{+4}}{\rightleftharpoons}} H3886 \tag{154}$$

**Table 6**
*Parameters for $^{13}C$-$^{18}O$-$^{18}O$ Clumped Isotopes*

| Symbol | Value | Reference/Note |
|---|---|---|
| $\Delta^{eq}_{49,CO_2}$ | $108776/T_K^2 + 477.14/T_K - 0.5954$ | Wang et al. (2004) |
| $\Delta^{eq}_{65,HCO_3^-}$ | [see Table 2] | – |
| $\Delta^{eq}_{65,CO_3^{2-}}$ | [see Table 2] | – |
| $\left({}^{49}R/{}^{49}R^*\right)^{eq}_{CO_2}$ | $\Delta^{eq}_{49,CO_2}/1000 + 1$ | – |
| $\left({}^{65}R/{}^{65}R^*\right)^{eq}_{HCO_3^-}$ | $\Delta^{eq}_{65,HCO_3^-}/1000 + 1$ | – |
| $\left({}^{65}R/{}^{65}R^*\right)^{eq}_{CO_3^{2-}}$ | $\Delta^{eq}_{65,CO_3^{2-}}/1000 + 1$ | – |
| ${}^{65}\alpha^{eq}_{CO_3^{2-}-HCO_3^-}$ | $\left({}^{65}R/{}^{65}R^*\right)^{eq}_{CO_3^{2-}} / \left({}^{65}R/{}^{65}R^*\right)^{eq}_{HCO_3^-}$ | – |
| ${}^{65}K_2$ | ${}^{65}\alpha^{eq}_{CO_3^{2-}-HCO_3^-} \cdot {}^{13}\alpha^{eq}_{CO_3^{2-}-HCO_3^-} \cdot {}^{18}\alpha^{eq}_{CO_3^{2-}-HCO_3^-} \cdot {}^{18}\alpha^{eq}_{CO_3^{2-}-HCO_3^-} \cdot K_2$ | – |
| ${}^{65}\chi$ | $\frac{1}{1+\frac{{}^{65}K_2}{[H^+]}}$ | – |
| ${}^{13-18-18}\mathrm{KIE}_{p''_{+1}}$ | $(11896.5529/T_K^2 - 84.3221/T_K - 0.168)/1000 + 1$ | Guo (2020) |
| ${}^{13-18-18}\mathrm{KIE}_{s''_{+1}}$ | $(-29208.4768/T_K^2 - 83.2994/T_K + 0.035)/1000 + 1$ | Guo (2020) |
| ${}^{13-18-18}\mathrm{KIE}_{p''_{+4}}$ | $(-6817.6067/T_K^2 + 92.9194/T_K - 0.517)/1000 + 1$ | Guo (2020) |
| ${}^{13-18-18}\mathrm{KIE}_{s''_{+4}}$ | $(-34709.15/T_K^2 - 125.3407/T_K + 0.409)/1000 + 1$ | Guo (2020) |
| $p''_{+1}, s''_{+1}$ | $p''_{+1} = \left({}^{13-18-18}\mathrm{KIE}_{p''_{+1}} \cdot c_{+1} \cdot b_{+1} \cdot a_{+1}\right)/k^2_{+1}$ | – |
| | $s''_{+1} = \left({}^{13-18-18}\mathrm{KIE}_{s''_{+1}} \cdot c_{+1} \cdot b_{+1} \cdot b_{+1}\right)/k^2_{+1}$ | – |
| $p''_{-1}, s''_{-1}$ | $p''_{-1} = p''_{+1} \cdot \left[\left({}^{47}R/{}^{47}R^*\right)^{eq}_{CO_2}\right] / \left[\left({}^{65}R/{}^{65}R^*\right)^{eq}_{HCO_3^-} \cdot K_1 \cdot {}^{13}\alpha^{eq}_{HCO_3^--CO_2} \cdot {}^{18}\alpha^{eq}_{HCO_3^--CO_2} \cdot {}^{18}\alpha^{eq}_{HCO_3^--H_2O}\right]$ | – |
| | $s''_{-1} = s''_{+1} \cdot \left[\left({}^{49}R/{}^{49}R^*\right)^{eq}_{CO_2}\right] / \left[\left({}^{65}R/{}^{65}R^*\right)^{eq}_{HCO_3^-} \cdot K_1 \cdot {}^{13}\alpha^{eq}_{HCO_3^--CO_2} \cdot {}^{18}\alpha^{eq}_{HCO_3^--CO_2} \cdot {}^{18}\alpha^{eq}_{HCO_3^--CO_2}\right]$ | – |
| $p''_{+4}, s''_{+4}$ | $p''_{+4} = \left({}^{13-18-18}\mathrm{KIE}_{p''_{+4}} \cdot c_{+4} \cdot b_{+4} \cdot a_{+4}\right)/k^2_{+4}$ | – |
| | $s''_{+4} = \left({}^{13-18-18}\mathrm{KIE}_{s''_{+4}} \cdot c_{+4} \cdot b_{+4} \cdot b_{+4}\right)/k^2_{+4}$ | – |
| $p''_{-4}, s''_{-4}$ | $p''_{-4} = p''_{+4} \cdot \left[\left({}^{47}R/{}^{47}R^*\right)^{eq}_{CO_2}\right] / \left[\left({}^{65}R/{}^{65}R^*\right)^{eq}_{HCO_3^-} \cdot K_1/K_w \cdot {}^{13}\alpha^{eq}_{HCO_3^--CO_2} \cdot {}^{18}\alpha^{eq}_{HCO_3^--CO_2} \cdot {}^{18}\alpha^{eq}_{HCO_3^--OH^-}\right]$ | – |
| | $s''_{-4} = s''_{+4} \cdot \left[\left({}^{49}R/{}^{49}R^*\right)^{eq}_{CO_2}\right] / \left[\left({}^{65}R/{}^{65}R^*\right)^{eq}_{HCO_3^-} \cdot K_1/K_w \cdot {}^{13}\alpha^{eq}_{HCO_3^--CO_2} \cdot {}^{18}\alpha^{eq}_{HCO_3^--CO_2} \cdot {}^{18}\alpha^{eq}_{HCO_3^--CO_2}\right]$ | – |

#### 4.4.2. ODEs

From the preceding reactions we obtain the following ODEs:

$$\begin{aligned}\frac{d[388]}{dt} =& -s''_{+1}[388] + \frac{1}{3}s''_{-1}[E3886]{}^{65}\chi[H] \\ & - s''_{+4}[388][6H] + \frac{1}{3}s''_{-4}[E3886]{}^{65}\chi\end{aligned} \tag{155}$$

$$\begin{aligned}\frac{d[E3886]}{dt} =& p''_{+1}[386]r_w - \frac{2}{3}p''_{-1}[E3886]{}^{65}\chi[H] \\ & + p''_{+4}[386][8H] - \frac{2}{3}p''_{-4}[E3886]{}^{65}\chi \\ & + s''_{+1}[388] - \frac{1}{3}s''_{-1}[E3886]{}^{65}\chi[H] \\ & + s''_{+4}[388][6H] - \frac{1}{3}s''_{-4}[E3886]{}^{65}\chi\end{aligned} \tag{156}$$

#### 4.4.3. Fraction of $HCO_3^-$ in the EIC

The derivation of ${}^{65}\chi$ is provided in Supplement S8 in Supporting Information S1 with the resulting expression provided in Table 6.

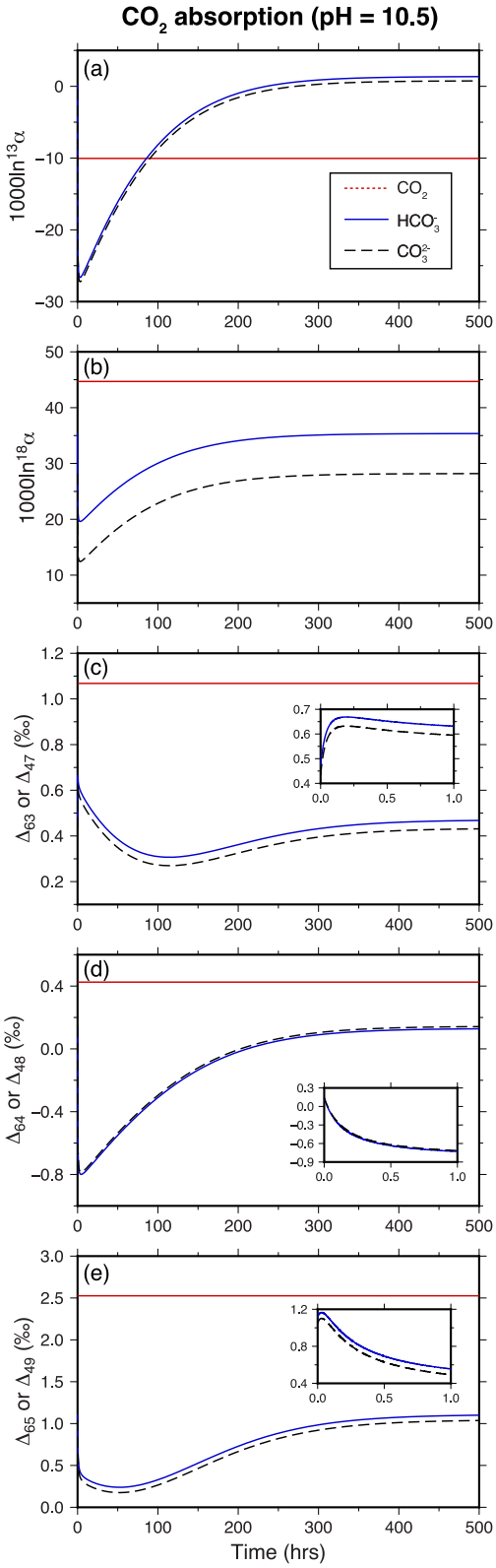


**Figure 3.** Behavior of the DIC-$H_2O$ model at 5°C and high pH using rate constants compiled in Tables 3–6. In this run, the dissolved inorganic carbon pool is initially equilibrated; then, the $CO_2$ is perturbed and held constant while the system adjusts to the new equilibrium.

#### 4.4.4. Rate Constants

The derivation of $p''$ and $s''$ rate constants is provided in Supplement S8 in Supporting Information S1 with results compiled in Table 6.

### 4.5. DIC-$H_2O$ Model Behavior

To demonstrate the behavior of the DIC-$H_2O$ model, we follow the approach used by Guo (2020) and show what happens when a high-pH solution absorbs $CO_2$ (Figure 3). We chose this scenario because it is relevant to the experimental results discussed in Section 5. In the simulation, the DIC pool (4 mM) is initially equilibrated and then the $CO_2$ concentration and its $\delta^{13}C$ are increased and held constant while the system adjusts to a new equilibrium. The run conditions differ from those of Guo (2020) in three ways: (a) our model neglects $^{17}O$ isotopologues, (b) we use a different set of equilibrium and kinetic parameters (Tables 3–6), and (c) we show results at $T = 5$°C and pH = 10.5 whereas Guo (2020) showed results at $T = 25$°C and pH = 9. A direct comparison between our model outputs and those of Guo (2020) using the same set of parameters is provided in Supplement S9 in Supporting Information S1.

Figure 3 shows how the isotopic compositions of $HCO_3^-$ and $CO_3^{2-}$ quickly respond to the change in $CO_2$ (as emphasized by the insets showing what happens in the first hour) and then gradually evolve to their respective equilibrium compositions on a timescale of about 500 hr. This timescale is consistent with that predicted by the analytical expression for the timescale to reach 99% oxygen isotope equilibration ($\tau_{99\%} \sim 685$ hr; Uchikawa & Zeebe, 2012).

The DIC-$H_2O$ model is useful for predicting the magnitude of disequilibrium effects and how different processes such as $CO_2$ absorption and degassing give rise to distinct signatures in the isotopic composition ($\delta^{13}C$, $\delta^{18}O$, $\Delta_{47}$, $\Delta_{48}$, and $\Delta_{49}$) of the aqueous solution (Guo, 2020). The DIC-$H_2O$ model has already been employed to identify and correct for KIEs in corals and other natural carbonate minerals but with the caveat that "the timing information in the model has no direct implication on the timescale of coral calcification process" because the $CO_2$ supply rate is treated as infinitely fast and there is no $CaCO_3$ outflux. (Bajnai et al., 2020). To more accurately model open-system laboratory experiments and natural environments, an open-system treatment with finite $CO_2$ and $CaCO_3$ fluxes is warranted. As we show below, such a treatment affects the range of expected KIEs and gives additional timing information such as how KIEs vary with crystal growth rate.

## 5. Combined Model and Application to Inorganic Calcite Precipitation Experiments

We can now combine the $CaCO_3$-DIC model from Section 3 and the DIC-$H_2O$ model from Section 4 into an open-system box model for the complete $CaCO_3$-DIC-$H_2O$ system. We refer to the general framework as "COAD," which is short for "carbon, oxygen, $\alpha$, $\Delta$." The model is applied to inorganic calcite precipitation experiments of Tang et al. (2014). This data set is particularly amenable to a box model because the experimental solutions were well-stirred (homogeneous) and the authors provided information regarding the magnitude and isotopic composition of DIC fluxes. The goals of this exercise are: (a) to provide the first example of a clumped isotope box model with a complete set of reaction kinetics that can be adapted to other situations and (b) to quantitatively evaluate the hypothesis by Tang

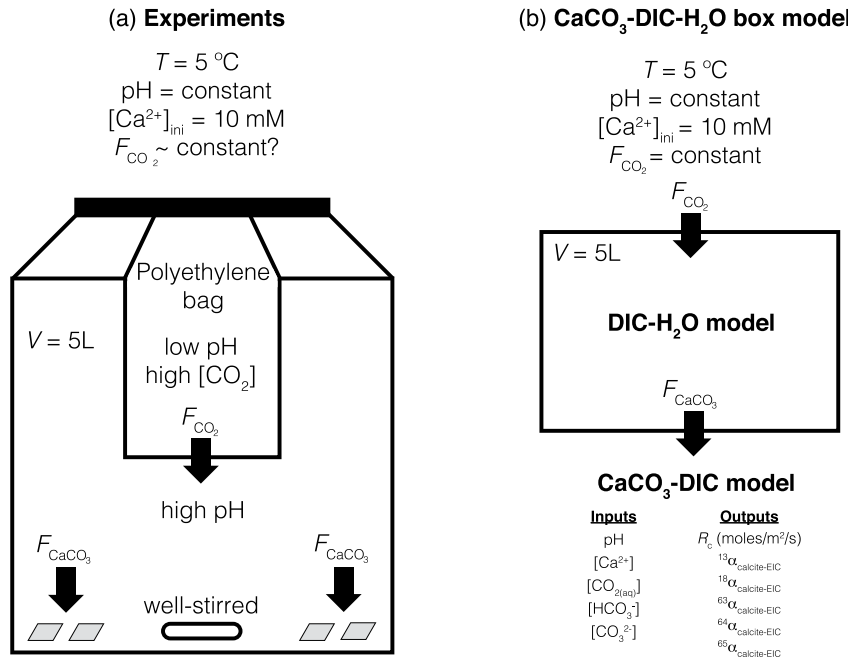


**Figure 4.** (a) Experimental setup used by Dietzel et al. (2009) and Tang et al. (2014). (b) Setup for the combined isotopic box model of the $CaCO_3$-DIC-$H_2O$ system.

et al. (2014) that extreme light isotope enrichments in their experiments are due to some combination of $CO_2$ diffusion through a membrane and the $CO_2$ hydroxylation reaction.

### 5.1. Summary of the Tang et al. (2014) Experiments

The experimental setup is shown in Figure 4a. A polyethylene (PE) container houses an inner solution with no $Ca^{2+}$ but high $CO_{2(aq)}$. The PE container is placed in an outer solution with 10 mM $CaCl_2$ and no DIC initially. The DIC is delivered to the outer solution by $CO_2$ diffusion through the PE membrane. The $CO_2$ flux varies between experiments because of differences in membrane thickness and in the pH of inner and outer solutions. The pH of the outer solution is held constant through the use of an autotitrator with NaOH as the titrant.

Tang et al. (2014) describe their experiments as consisting of two stages. During Stage I, $CO_2$ diffuses from the inner to outer solution and the concentration of DIC in the outer solution increases monotonically until a critical saturation is reached for spontaneous calcite precipitation. During Stage II, the outer solution experiences both a $CO_2$ influx and $CaCO_3$ outflux. Stage II is characterized by a short period of rapid $CaCO_3$ nucleation and growth followed by a prolonged period of slower growth under nearly steady state conditions.

A modified version of the experimental parameters and results of Tang et al. (2014) is given in Table 7. The flux of $CO_2$ into solution during Stage I was calculated from [DIC] at the end of Stage I and the duration of Stage I ($t_1$). The flux of $CaCO_3$ was calculated from the moles of $CaCO_3$ precipitated ($M$) and duration of Stage II ($t_2$). The surface area (SA) normalized growth rate of $CaCO_3$ (moles $m^{-2}$ $s^{-1}$) was calculated by Tang et al. (2014) using a specific SA for calcite based on particle size distributions. From the reported growth rates, the total reactive SA of crystals at the end of the experiments span the range of 0.056–0.209 $m^2$. These represent maximum values since the starting surface area is 0 $m^2$.

### 5.2. Combined Model Setup

The open-system model deals only with Stage II and involves two fluxes: $F_{CO_2}$ and $F_{CaCO_3}$ (both in mol $s^{-1}$) (Figure 4b). For simplicity, we consider the reactive SA as constant but adjustable within the range of 0 to 0.209 $m^2$. We find that a value of 0.01 $m^2$ yields generally good agreement between the steady state $F_{CO_2}$ (or $F_{CaCO_3}$) and

**Table 7**
*Experimental Data From Dietzel et al. (2009) and Tang et al. (2014) Used to Constrain the Input Parameters (T, pH, [$Ca^{2+}$]) and Adjustable Parameters ($F_{CO_2}$ and SA) Used in the Model*

| Exp[a] | T (°C) | $pH_{out}$ | $t_1$ (h) | $t_2$ (h) | $t_{tot}$ (h) | M (mmoles) | $[Ca^{2+}]_{ini}$ (mM) | [DIC][b] (mM) | $F_{CO_2}$[c] (mmol/h) | $F_{CaCO_3}$[d] (mmol/h) | SA $m^2$ | $\log_{10}R$ moles/$m^2$/s | 1000ln$\alpha$ | $\Delta_{47}$ ARF |
|---|---|---|---|---|---|---|---|---|---|---|---|---|---|---|
| 1 | 5 | 9 | 194 | 647 | 841 | 5.8 | 10.1 | 0.24 | 0.006 | 0.009 | 0.059 | −7.38 | 26.75 | 0.733 |
| 2 | 5 | 9 | 186 | 402 | 588 | 5.2 | 9.9 | 0.24 | 0.006 | 0.013 | 0.073 | −7.31 | 28.23 | 0.735 |
| 3 | 5 | 9 | 162 | 223 | 385 | 9.6 | 10.5 | 0.33 | 0.010 | 0.043 | 0.188 | −7.20 | 29.49 | 0.748 |
| 4 | 5 | 10 | 119 | 309 | 428 | 6.9 | 9.9 | 0.05 | 0.002 | 0.022 | 0.112 | −7.26 | 14.09 | 0.962 |
| 5 | 5 | 8.5 | 438 | 336 | 774 | 3.7 | 10.2 | 0.53 | 0.006 | 0.011 | 0.056 | −7.27 | 31.51 | 0.787 |
| 6 | 5 | 10.5 | 48 | 187 | 235 | 12.4 | 92.5 | 0.04 | 0.004 | 0.066 | 0.230 | −7.10 | 13.07 | 1.065 |
| 7 | 5 | 8.3 | 72 | 26 | 98 | 6.6 | 10.0 | 2.15 | 0.149 | 0.254 | 0.164 | −6.37 | 31.22 | 0.765 |
| 9 | 5 | 8.3 | 127 | 65 | 192 | 4.8 | 10.3 | 1.6 | 0.063 | 0.074 | 0.107 | −6.72 | 31.78 | 0.753 |
| 10 | 5 | 8.3 | 61 | 51 | 112 | 9.3 | 9.9 | 1.95 | 0.160 | 0.182 | 0.209 | −6.62 | 30.99 | 0.752 |

[a]Experiment numbers from Dietzel et al. (2009). [b][DIC] at the end of Stage I. c$F_{CO_2}$ during Stage I. d$F_{CaCO_3}$ during Stage II.

the measured surface area normalized growth rates across the experimental data set as a whole. Additional details regarding the treatments of $F_{CO_2}$ and $F_{CaCO_3}$ are described individually below.

### 5.2.1. $CO_2$ Flux

It is important to consider the isotopic composition of $CO_2$ as it enters solution during Stage I and throughout Stage II. We assume that the $CO_{2(aq)}$ in the inner solution is isotopically equilibrated with water. Under the experimental conditions (5°C and pH of inner solution between 7.3 and 8.1), the equilibration time for oxygen and clumped isotopes ($t_{99\%}$) ranges from 6 to 35 hr (Affek, 2013; Clog et al., 2015; Staudigel & Swart, 2018; Uchikawa & Zeebe, 2012). Tang et al. (2014) did not report the pre-experiment dwell time and whether or not it was sufficient to ensure isotopic equilibration. Additional fractionation may occur during $CO_{2(g)}$ transport through the PE membrane. This could potentially lead to lower $\delta^{18}O$ and higher $\Delta_{47}$ values (Eiler and Schauble, 2004).

### 5.2.2. $CaCO_3$ Flux

The precipitation of $CaCO_3$ constitutes a sink of EIC isotopologues (recall that EIC refers to "equilibrated inorganic carbon," or $HCO_3^-$ + $CO_3^{2-}$) that affects the isotopic composition of residual EIC. Chen et al. (2018) provided the $CaCO_3$ flux terms for carbon and oxygen isotopes. Here, we derive the $CaCO_3$ sink term for E3866. To begin, we have the following definition:

$$\left(\frac{^{63}R}{^{63}R^*}\right) = \frac{\left(\frac{[3866]}{[2666]}\right)}{\left(\frac{[3666]}{[2666]}\right)\left(\frac{[2866]}{[2666]}\right)}. \tag{157}$$

Next, we define a kinetic clumped isotope fractionation factor:

$$^{63}\alpha_{CaCO_3-EIC} = \frac{\left(\frac{^{63}R}{^{63}R^*}\right)_{CaCO_3}}{\left(\frac{^{63}R}{^{63}R^*}\right)_{EIC}} = \frac{\left[\frac{\left(\frac{[Ca3866]}{[Ca2666]}\right)}{\left(\frac{[Ca3666]}{[Ca2666]}\right)\left(\frac{[Ca2866]}{[Ca2666]}\right)}\right]}{\left[\frac{\left(\frac{[E3866]}{[E2666]}\right)}{\left(\frac{[E3666]}{[E2666]}\right)\left(\frac{[E2866]}{[E2666]}\right)}\right]}, \tag{158}$$

which upon rearrangement leads to

$$^{63}\alpha_{CaCO_3-EIC} = \frac{\left(\frac{[Ca3866]}{[Ca2666]}\right)}{\left(\frac{[E3866]}{[E2666]}\right)} \cdot \frac{\left(\frac{[E3666]}{[E2666]}\right)}{\left(\frac{[Ca3666]}{[Ca2666]}\right)} \cdot \frac{\left(\frac{[E2866]}{[E2666]}\right)}{\left(\frac{[Ca2866]}{[Ca2666]}\right)} = \frac{\left(\frac{[Ca3866]}{[Ca2666]}\right)}{\left(\frac{[E3866]}{[E2666]}\right)} \cdot {}^{13}\alpha_{EIC-CaCO_3} \cdot {}^{18}\alpha_{EIC-CaCO_3}. \tag{159}$$

Solving for [Ca3866] leads to

$$[\mathrm{Ca3866}] = [\mathrm{Ca2666}] \cdot \frac{[\mathrm{E3866}]}{[\mathrm{E2666}]} \cdot {}^{63}\alpha_{\mathrm{CaCO_3-EIC}} \cdot {}^{13}\alpha_{\mathrm{CaCO_3-EIC}} \cdot {}^{18}\alpha_{\mathrm{CaCO_3-EIC}}. \tag{160}$$

Considering this expression in terms of the flux of $CaCO_3$, we can write:

$$\frac{\mathrm{d}[\mathrm{Ca3866}]}{\mathrm{dt}} = \frac{F_{\mathrm{CaCO_3}}}{V} \cdot \frac{[\mathrm{E3866}]}{[\mathrm{E2666}]} \cdot {}^{63}\alpha_{\mathrm{CaCO_3-EIC}} \cdot {}^{13}\alpha_{\mathrm{CaCO_3-EIC}} \cdot {}^{18}\alpha_{\mathrm{CaCO_3-EIC}}. \tag{161}$$

Finally, the effect of calcite precipitation on the clumped isotope composition of residual EIC is given by

$$\frac{\mathrm{d}[\mathrm{Ca3866}]}{\mathrm{dt}} = -\frac{\mathrm{d}[\mathrm{E3866}]}{\mathrm{dt}}. \tag{162}$$

The clumped isotope composition of calcite relative to EIC is calculated from the $CaCO_3$-DIC model.

Similar expressions can be derived for $^{18}O$-$^{18}O$ and $^{13}C$-$^{18}O$-$^{18}O$ clumped isotopes:

$$\frac{\mathrm{d}[\mathrm{E2886}]}{\mathrm{dt}} = -\frac{F_{\mathrm{CaCO_3}}}{V} \cdot \frac{[\mathrm{E2886}]}{[\mathrm{E2666}]} \cdot {}^{64}\alpha_{\mathrm{CaCO_3-EIC}} \cdot {}^{18}\alpha_{\mathrm{CaCO_3-EIC}} \cdot {}^{18}\alpha_{\mathrm{CaCO_3-EIC}} \tag{163}$$

and

$$\frac{\mathrm{d}[\mathrm{E3886}]}{\mathrm{dt}} = -\frac{F_{\mathrm{CaCO_3}}}{V} \cdot \frac{[\mathrm{E3886}]}{[\mathrm{E2666}]} \cdot {}^{65}\alpha_{\mathrm{CaCO_3-EIC}} \cdot {}^{13}\alpha_{\mathrm{CaCO_3-EIC}} \cdot {}^{18}\alpha_{\mathrm{CaCO_3-EIC}} \cdot {}^{18}\alpha_{\mathrm{CaCO_3-EIC}}. \tag{164}$$

### 5.3. Governing Equations

The Tang et al. (2014) experiments are modeled by solving the following system of equations:

$$\frac{\mathrm{d}[266]}{\mathrm{dt}} = \{\mathrm{rxn\ terms, Eq.92}\} + \frac{F_{\mathrm{CO_2}}}{V} \tag{165}$$

$$\frac{\mathrm{d}[\mathrm{E2666}]}{\mathrm{dt}} = \{\mathrm{rxn\ terms, Eq.93}\} - \frac{F_{\mathrm{CaCO_3}}}{V} \tag{166}$$

$$\frac{\mathrm{d}[366]}{\mathrm{dt}} = \{\mathrm{rxn\ terms, Eq.94}\} + \frac{F_{\mathrm{CO_2}} \cdot {}^{13}R_{\mathrm{CO_2}}}{V} \tag{167}$$

$$\frac{\mathrm{d}[\mathrm{E3666}]}{\mathrm{dt}} = \{\mathrm{rxn\ terms, Eq.95}\} - \frac{F_{\mathrm{CaCO_3}}}{V} \cdot \frac{[\mathrm{E3666}]}{[\mathrm{E2666}]} \cdot {}^{13}\alpha_{\mathrm{CaCO_3-EIC}} \tag{168}$$

$$\frac{\mathrm{d}[286]}{\mathrm{dt}} = \{\mathrm{rxn\ terms, Eq.96}\} + \frac{F_{\mathrm{CO_2}} \cdot {}^{18}R_{\mathrm{CO_2}}}{V} \tag{169}$$

$$\frac{\mathrm{d}[\mathrm{E2866}]}{\mathrm{dt}} = \{\mathrm{rxn\ terms, Eq.97}\} - \frac{F_{\mathrm{CaCO_3}}}{V} \cdot \frac{[\mathrm{E2866}]}{[\mathrm{E2666}]} \cdot {}^{18}\alpha_{\mathrm{CaCO_3-EIC}} \tag{170}$$

$$\frac{\mathrm{d}[386]}{\mathrm{dt}} = \{\mathrm{rxn\ terms, Eq.127}\} + \frac{F_{\mathrm{CO_2}} \cdot {}^{47}R_{\mathrm{CO_2}}}{V} \tag{171}$$

$$\frac{\mathrm{d}[\mathrm{E3866}]}{\mathrm{dt}} = \{\mathrm{rxn\ terms, Eq.128}\} - \frac{F_{\mathrm{CaCO_3}}}{V} \cdot \frac{[\mathrm{E3866}]}{[\mathrm{E2666}]} \cdot {}^{63}\alpha_{\mathrm{CaCO_3-EIC}} \cdot {}^{13}\alpha_{\mathrm{CaCO_3-EIC}} \cdot {}^{18}\alpha_{\mathrm{CaCO_3-EIC}} \tag{172}$$

$$\frac{\mathrm{d}\left[\mathrm{Ca^{2+}}\right]}{\mathrm{dt}} = -\frac{F_{\mathrm{CaCO_3}}}{V} \tag{173}$$

Since we treat the experiments as "seeded" we initialize the model with $[Ca^{2+}] = 10$ mM and enough DIC so that $\Omega = 7$, which is representative of the $\Omega$ at the start of Stage II of the experiments (Dietzel et al., 2009). The $CO_2$ that enters into solution gets converted to $HCO_3^-$ according to the $CO_2$ hydration and hydroxylation reactions,

leading to light isotope enrichment of $HCO_3^-$, and calcite grows at a rate that depends on $[Ca^{2+}]$ and $[CO_3^{2-}]$. The Matlab script that accompanies this article is subdivided into the following sequence of operations (pseudocode):

1. Specify $T$, pH, salinity, $V$, $[Ca^{2+}]$, the initial $\Omega$, the crystal reactive SA, and $F_{CO_2}$. Calculate $[CO_3^{2-}]$ from $[Ca^{2+}]$ and $\Omega$.
2. Calculate $K_1$, $K_2$, $K_w$, and $K_{sp}$ as functions of $T$ and salinity.
3. Calculate [DIC] and DIC speciation from $[CO_3^{2-}]$ and pH (Zeebe & Wolf-Gladrow, 2001).
4. Calculate the equilibrium carbon, oxygen, and clumped isotope fractionation factors as functions of $T$.
5. Calculate the forward $k$ values for all reactions.
6. Calculate the backward $k$ values using the forward $k$'s and equilibrium constraints.
7. Calculate the equilibrium isotopologue concentrations.
8. Specify the isotopic composition of $F_{CO_2}$. In the default model, the incoming $CO_2$ is equilibrated with water.
9. Solve the system of coupled ODEs (Equations 165–173). At each time step, the $HCO_3^-$ and $CO_3^{2-}$ isotopologue concentrations are calculated from the EIC isotopologue concentrations using the $\chi$ values. These are then used as inputs into the $CaCO_3$-DIC model, which returns the SA normalized growth rate as well as the pH- and growth rate-dependent ${}^{13}\alpha_{CaCO_3-EIC}$, ${}^{18}\alpha_{CaCO_3-EIC}$, ${}^{63}\alpha_{CaCO_3-EIC}$, ${}^{64}\alpha_{CaCO_3-EIC}$, and ${}^{65}\alpha_{CaCO_3-EIC}$ values. The growth rate is multiplied by the reactive SA (0.01 $m^2$ for this simulation) to get $F_{CaCO_3}$, which feeds back into the ODEs, and the calculation is repeated until steady state is reached.

### 5.4. Model Behavior

An example showing the behavior of the model run to steady state is shown in Figure 5. The $CO_2$ flux is held constant at 0.01 mmol/hr (Figure 5a), which is in the middle of the range of the Tang et al. (2014) experiments. The flux of $CaCO_3$ is initially high and decreases monotonically until it exactly balances with the specified flux of $CO_2$ (Figure 5b). The time required to reach a steady state $F_{CaCO_3}$ depends on $F_{CO_2}$, with low values requiring longer simulation times. The oxygen isotope composition of DIC is initially equilibrated and then $1000\ln{}^{18}\alpha$ steadily decreases due to the $CO_2$ hydration and hydroxylation reactions (Figure 5c). After several hours, the system reaches a steady state composition that is far from equilibrium. For clumped isotopes, the $CO_2$ becomes more ordered (higher $\Delta_{47}$; Figure 5d) and the DIC species also become more ordered (higher $\Delta_{63}$; Figure 5e) during $CO_2$ hydration and hydroxylation.

### 5.5. Model Application

Outputs from the model are compared to the Tang et al. (2014) data in Figures 6a and 6b. Each point on a model curve represents the *steady state* isotopic composition for the specified pH and $F_{CO_2}$. Overall, the model fits the data well, which is noteworthy given that we treat the EFFs and KFFs as "known" and the only adjustable parameter is the reactive surface area of crystals. For both oxygen and clumped isotopes, there is an indication that the model may be underestimating the oxygen and perhaps also the clumped isotope KIEs at the highest pH values. However, given the ~3‰ spread in $\delta^{18}O$ in the replicate experiments at pH = 9.0, and the 0.05‰ variability in $\Delta_{47}$ among inorganic calibrations at a given $T$ (see Figure 5 of Kelson et al., 2017), it is unclear how much emphasis to place on the data-model disagreement at high pH.

The range in solution pH (8.3–10.5) and crystal growth rate ($\log_{10}R$ = –6.37 to –7.38 mol $m^{-2}$ $s^{-1}$) resulted in an 18.7‰ range in $1000\ln{}^{18}\alpha$ and 0.33 range in $\Delta_{63}$ (Tang et al., 2014). Although most of this variability can be explained by $CO_2$ exchange with water in the DIC-$H_2O$ system, it is also clear that the $CO_2$ and $CaCO_3$ fluxes have a strong influence on the KIEs by modulating the reversibility of the $CO_2$ hydration and hydroxylation reactions. For a given $F_{CO_2}$, higher pH yields larger KIEs, and for a given pH, a higher $F_{CO_2}$ or $F_{CaCO_3}$ promotes unidirectional reaction and larger KIEs. It is thus important to account for these fluxes even though the KIEs attending the crystal growth reactions may be relatively minor.

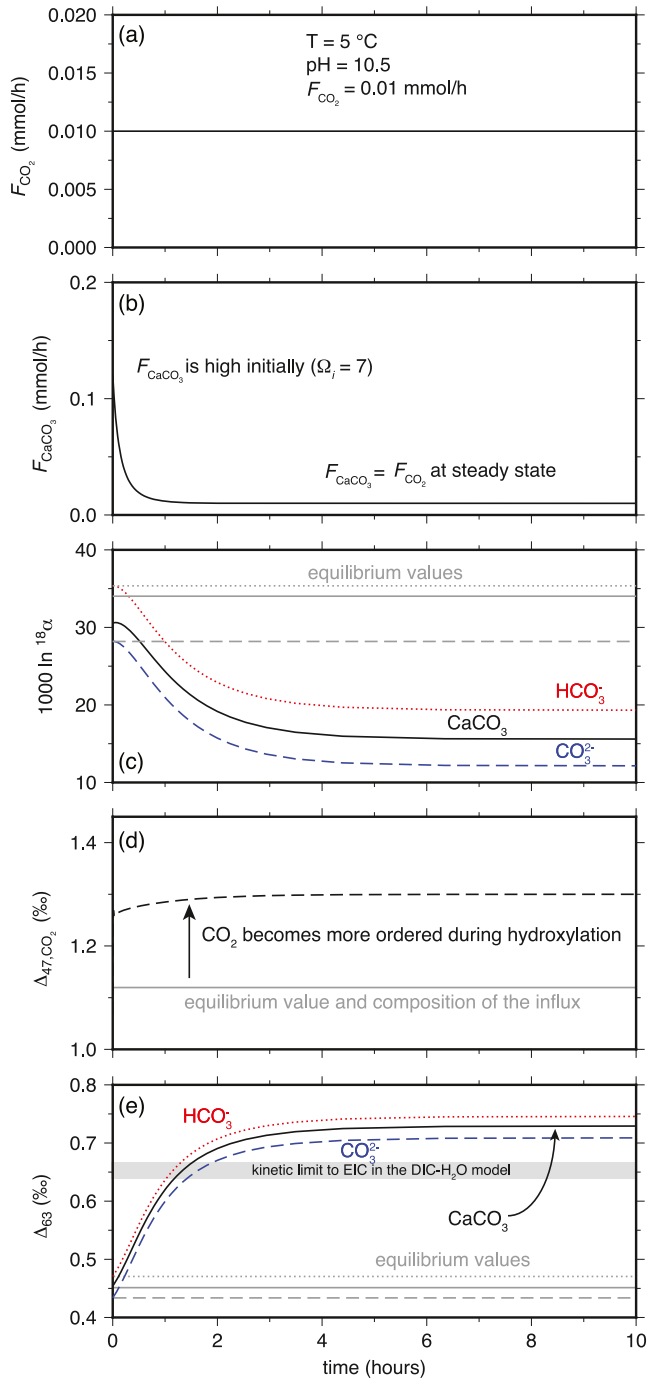


**Figure 5.** $CaCO_3$-DIC-$H_2O$ box model run showing the time evolution of the system. (a) $F_{CO_2}$ is held constant throughout. (b) $F_{CaCO_3}$ at each time step is calculated from the $CaCO_3$-DIC model based on the degree of supersaturation. Initially, $\Omega = 7$ and it decreases monotonically until $F_{CaCO_3} = F_{CO_2}$. In this example, the steady state $F_{CaCO_3}$ translates to $\log_{10}R = -6.6$ mol/m$^2$/s. (c) The oxygen isotope composition of $HCO_3^-$ and $CO_3^{2-}$ decrease due to kinetic effects attending $CO_2$ hydration and hydroxylation. $CaCO_3$ inherits the light composition of $HCO_3^-$ and $CO_3^{2-}$ plus an additional fractionation attending the crystal growth reaction. (d) The $\Delta_{47}$ of $CO_{2(aq)}$ increases due to the hydration and hydroxylation reactions. (e) The $\Delta_{63}$ of $HCO_3^-$ and $CO_3^{2-}$ increase due to KIEs attending the $CO_2$ hydration and hydroxylation reactions (gray horizontal bar) as well as the increase in $\Delta_{47}$ of $CO_{2(aq)}$. Calcite growth is fast enough for it to (nearly) inherit the clumped isotope composition of the weighted sum of $HCO_3^-$ and $CO_3^{2-}$.

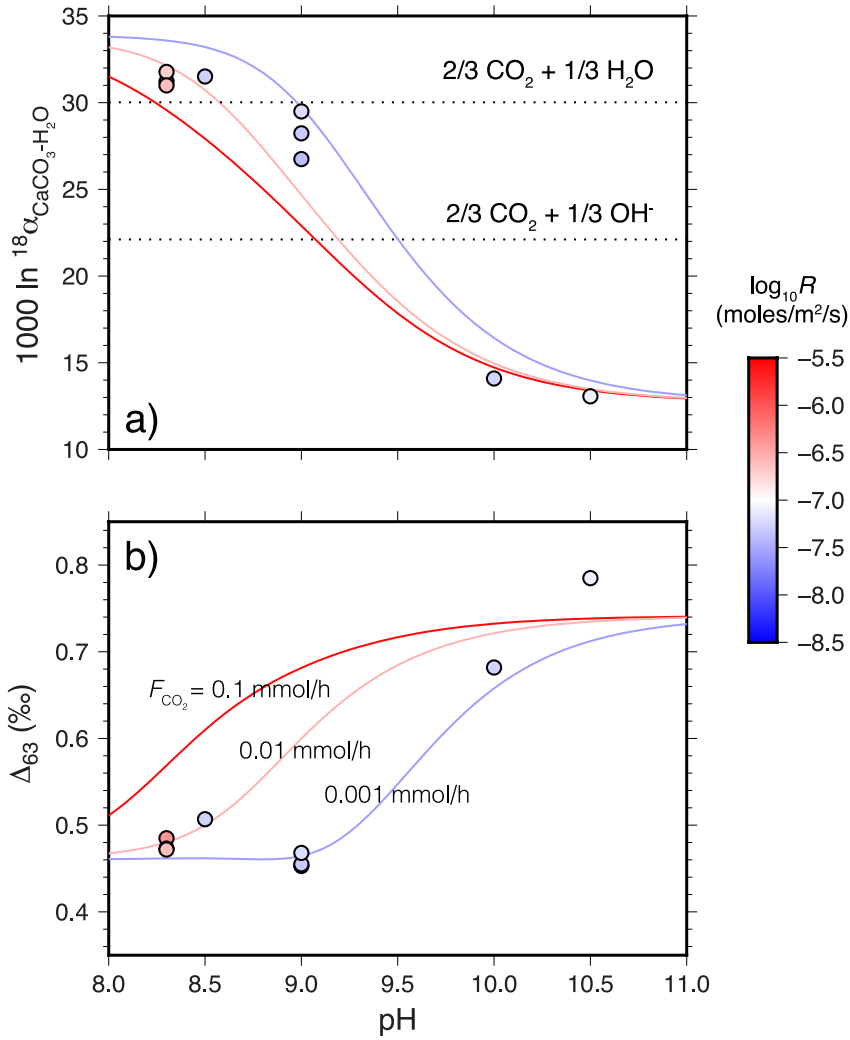


**Figure 6.** Model outputs compared to (a) oxygen isotope results and (b) clumped isotope results. The model is in good overall agreement with the data and shows the strong influence of growth rate on the KIEs. Note that the data from Tang et al. (2014) have been converted from $\Delta_{47}$ (absolute reference frame) to $\Delta_{63}$ using the acid fractionation factor of 0.28‰ (Tripati et al., 2015).

## 6. Summary and Future Directions

KIEs are ubiquitous in inorganic and biogenic carbonates. Open-system, reactive-transport models, and box models have been useful for understanding the cause(s) of kinetic $\delta^{13}C$ and $\delta^{18}O$ effects in corals (Adkins et al., 2003; Chen et al., 2018), foraminifers (Zeebe et al., 1999), speleothems (Guo & Zhou, 2019a; Hansen et al., 2017; Sade et al., 2022), and alkaline travertines (Christensen et al., 2021). Kinetic clumped isotope effects hold additional information about the conditions of carbonate formation, but only recently has there been sufficient information regarding clumped isotope KFFs to extend the models to $\Delta_{63}$, $\Delta_{64}$, and $\Delta_{65}$.

The recent experimental and analytical developments motivated us to update and expand an ion-by-ion model that describes KIEs in the $CaCO_3$-DIC system (Watkins & Hunt, 2015) to include $^{18}O$-$^{18}O$ ($\Delta_{64}$) and $^{13}C$-$^{18}O$-$^{18}O$ ($\Delta_{65}$) clumped isotopes. We similarly expanded an existing model of the DIC-$H_2O$ system (Uchikawa et al., 2021) to include $^{18}O$-$^{18}O$ and $^{13}C$-$^{18}O$-$^{18}O$ clumped isotopes. The two models are built on a common framework that tracks the abundances of isotopologues and we showed how the two models can be coupled in order to describe KIEs in the full $CaCO_3$-DIC-$H_2O$ system.

We applied the combined model ("COAD") to the inorganic calcite precipitation experiments of Tang et al. (2014). With only one adjustable parameter (the reactive surface area of calcite), the model is successful at explaining

their $1000\ln^{18}\alpha$ and $\Delta_{47}$ trends versus growth rate and pH. The model reveals that kinetic isotope effects from DIC-$H_2O$ exchange are strongly modulated by crystal growth rate and that including such growth rate effects will be important to future applications.

The COAD model enables one to calculate the $\delta^{13}C$, $\delta^{18}O$, $\Delta_{63}$, $\Delta_{64}$, and $\Delta_{65}$ of calcite under nonequilibrium conditions and is readily adaptable to other situations involving $CO_2$ absorption (e.g., corals, foraminifera, and high-pH travertines) or $CO_2$ degassing (e.g., speleothems, low-pH travertines, and cryogenic carbonates) and/or mixing with other DIC sources. We anticipate this model framework being useful for guiding future experiments, informing carbonate sample collection strategies, and interpreting paleoclimate records.

## Data Availability Statement

Matlab scripts used to produce some of the figures herein are available on GitHub (https://github.com/jwatkins529/COAD_Box_Model) and Zenodo (https://doi.org/10.5281/zenodo.6131547).

**Acknowledgments**
We are grateful to many colleagues for discussions and recent publications that underlie our understanding of the work presented here. In particular, we thank Don DePaolo, Kate Huntington, Casey Saenger, Aradhna Tripati, Jamie Lucarelli, and Zeeshan Parvez for many discussions surrounding $\Delta_{48}$ and the box model. We thank Weifu Guo for help on the DIC-$H_2O$ model comparison in Supplement S9 in Supporting Information S1; We thank Ellen Olsen for help in compiling and reviewing the KFFs; We thank Philip Staudigel, an anonymous reviewer, and the AE for guidance toward improving the quality and clarity of the manuscript. J. M. Watkins was supported by the National Science Foundation under NSF-CAREER Grant No. EAR1749183.

## References

Adkins, J., Boyle, E., Curry, W., & Lutringer, A. (2003). Stable isotopes in deep-sea corals and a new mechanism for "vital effects". *Geochimica et Cosmochimica Acta*, *67*(6), 1129–1143. https://doi.org/10.1016/s0016-7037(02)01203-6

Affek, H. P. (2013). Clumped isotopic equilibrium and the rate of isotope exchange between $CO_2$ and water. *American Journal of Science*, *313*(4), 309–325. https://doi.org/10.2475/04.2013.02

Affek, H. P., & Zaarur, S. (2014). Kinetic isotope effect in $CO_2$ degassing: Insight from clumped and oxygen isotopes in laboratory precipitation experiments. *Geochimica et Cosmochimica Acta*, *143*, 319–330. https://doi.org/10.1016/j.gca.2014.08.005

Bajnai, D., Fiebig, J., Tomašových, A., Garcia, S. M., Rollion-Bard, C., Raddatz, J., et al. (2018). Assessing kinetic fractionation in brachiopod calcite using clumped isotopes. *Scientific Reports*, *8*(1), 1–12. https://doi.org/10.1038/s41598-017-17353-7

Bajnai, D., Guo, W., Spötl, C., Coplen, T. B., Methner, K., Löffler, N., et al. (2020). Dual clumped isotope thermometry resolves kinetic biases in carbonate formation temperatures. *Nature Communications*, *11*(1), 1–9. https://doi.org/10.1038/s41467-020-17501-0

Beck, W. C., Grossman, E. L., & Morse, J. W. (2005). Experimental studies of oxygen isotope fractionation in the carbonic acid system at 15°, 25°, and 40°C. *Geochimica et Cosmochimica Acta*, *69*(14), 3493–3503. https://doi.org/10.1016/j.gca.2005.02.003

Bigeleisen, J., & Mayer, M. G. (1947). Calculation of equilibrium constants for isotopic exchange reactions. *The Journal of Chemical Physics*, *15*(5), 261–267. https://doi.org/10.1063/1.1746492

Bottinga, Y. (1968). Calculation of fractionation factors for carbon and oxygen isotopic exchange in the system calcite-carbon dioxide-water. *The Journal of Physical Chemistry*, *72*(3), 800–808. https://doi.org/10.1021/j100849a008

Candelier, Y., Minoletti, F., Probert, I., & Hermoso, M. (2013). Temperature dependence of oxygen isotope fractionation in coccolith calcite: A culture and core top calibration of the genus Calcidiscus. *Geochimica et Cosmochimica Acta*, *100*, 264–281. https://doi.org/10.1016/j.gca.2012.09.040

Chen, S., Gagnon, A. C., & Adkins, J. F. (2018). Carbonic anhydrase, coral calcification and a new model of stable isotope vital effects. *Geochimica et Cosmochimica Acta*, *236*, 179–197. https://doi.org/10.1016/j.gca.2018.02.032

Christensen, J. N., Watkins, J. M., Devriendt, L. S., DePaolo, D. J., Conrad, M. E., Voltolini, M., et al. (2021). Isotopic fractionation accompanying $CO_2$ hydroxylation and carbonate precipitation from high pH waters at the Cedars, California, USA. *Geochimica et Cosmochimica Acta*, *301*, 91–115. https://doi.org/10.1016/j.gca.2021.01.003

Clark, I. D., & Fontes, J.-C. (1990). Paleoclimatic reconstruction in northern Oman based on carbonates from hyperalkaline groundwaters. *Quaternary Research*, *33*(3), 320–336. https://doi.org/10.1016/0033-5894(90)90059-t

Clark, I. D., Fontes, J.-C., & Fritz, P. (1992). Stable isotope disequilibria in travertine from high pH waters: Laboratory investigations and field observations from Oman. *Geochimica et Cosmochimica Acta*, *56*(5), 2041–2050. https://doi.org/10.1016/0016-7037(92)90328-g

Clog, M., Stolper, D., & Eiler, J. M. (2015). Kinetics of $CO_{2(g)}$-$H_2O_{(l)}$ isotopic exchange, including mass 47 isotopologues. *Chemical Geology*, *395*, 1–10. https://doi.org/10.1016/j.chemgeo.2014.11.023

Coplen, T. B. (2007). Calibration of the calcite–water oxygen-isotope geothermometer at Devils Hole, Nevada, a natural laboratory. *Geochimica et Cosmochimica Acta*, *71*(16), 3948–3957. https://doi.org/10.1016/j.gca.2007.05.028

Daëron, M., Drysdale, R. N., Peral, M., Huyghe, D., Blamart, D., Coplen, T. B., et al. (2019). Most Earth-surface calcites precipitate out of isotopic equilibrium. *Nature Communications*, *10*(1), 1–7. https://doi.org/10.1038/s41467-019-08336-5

Dennis, K. J., & Schrag, D. P. (2010). Clumped isotope thermometry of carbonatites as an indicator of diagenetic alteration. *Geochimica et Cosmochimica Acta*, *74*(14), 4110–4122. https://doi.org/10.1016/j.gca.2010.04.005

DePaolo, D. J. (2011). Surface kinetic model for isotopic and trace element fractionation during precipitation of calcite from aqueous solutions. *Geochimica et Cosmochimica Acta*, *75*(4), 1039–1056. https://doi.org/10.1016/j.gca.2010.11.020

Devriendt, L. S., McGregor, H. V., & Chivas, A. R. (2017b). Ostracod calcite records the $^{18}O/^{16}O$ ratio of the bicarbonate and carbonate ions in water. *Geochimica et Cosmochimica Acta*, *214*, 30–50. https://doi.org/10.1016/j.gca.2017.06.044

Devriendt, L. S., Watkins, J. M., & McGregor, H. V. (2017a). Oxygen isotope fractionation in the $CaCO_3$-DIC-$H_2O$ system. *Geochimica et Cosmochimica Acta*, *214*, 115–142. https://doi.org/10.1016/j.gca.2017.06.022

Dietzel, M., Tang, J., Leis, A., & Köhler, S. J. (2009). Oxygen isotopic fractionation during inorganic calcite precipitation – Effects of temperature, precipitation rate and pH. *Chemical Geology*, *268*(1), 107–115. https://doi.org/10.1016/j.chemgeo.2009.07.015

DOE. (1994). *Handbook of Methods for the Analysis of the Various Variables of the Carbon Dioxide System in Seawater* (Vol. 2). Oak Ridge National Laboratory. ORNL/CDIAC-74.

Eiler, J. M. (2007). "Clumped-isotope" geochemistry – The study of naturally-occurring, multiply-substituted isotopologues. *Earth and Planetary Science Letters*, *262*(3), 309–327. https://doi.org/10.1016/j.epsl.2007.08.020

Eiler, J. M., & Schauble, E. (2004). $^{18}O^{13}C^{16}O$ in Earth's atmosphere. *Geochimica et Cosmochimica Acta*, *68*(23), 4767–4777. https://doi.org/10.1016/j.gca.2004.05.035

Erez, J. (2003). The source of ions for biomineralization in foraminifera and their implications for paleoceanographic proxies. *Reviews in Mineralogy and Geochemistry*, *54*(1), 115–149. https://doi.org/10.1515/9781501509346-010

Falk, E., Guo, W., Paukert, A., Matter, J., Mervine, E., & Kelemen, P. (2016). Controls on the stable isotope compositions of travertine from hyperalkaline springs in Oman: Insights from clumped isotope measurements. *Geochimica et Cosmochimica Acta*, *192*, 1–28. https://doi.org/10.1016/j.gca.2016.06.026

Fiebig, J., Bajnai, D., Löffler, N., Methner, K., Krsnik, E., Mulch, A., & Hofmann, S. (2019). Combined high-precision $\delta_{48}$ and $\delta_{47}$ analysis of carbonates. *Chemical Geology*, *522*, 186–191. https://doi.org/10.1016/j.chemgeo.2019.05.019

Fiebig, J., Daëron, M., Bernecker, M., Guo, W., Schneider, G., Boch, R., et al. (2021). Calibration of the dual clumped isotope thermometer for carbonates. *Geochimica et Cosmochimica Acta*, *312*, 235–256. https://doi.org/10.1016/j.gca.2021.07.012

Gabitov, R. I., Watson, E. B., & Sadekov, A. (2012). Oxygen isotope fractionation between calcite and fluid as a function of growth rate and temperature: An *in situ* study. *Chemical Geology*, *306*, 92–102. https://doi.org/10.1016/j.chemgeo.2012.02.021

Ghosh, P., Adkins, J., Affek, H., Balta, B., Guo, W., Schauble, E. A., et al. (2006). $^{13}C$–$^{18}O$ bonds in carbonate minerals: A new kind of paleothermometer. *Geochimica et Cosmochimica Acta*, *70*(6), 1439–1456. https://doi.org/10.1016/j.gca.2005.11.014

Guo, W. (2008). *Carbonate clumped isotope thermometry: Application to carbonaceous chondrites & effects of kinetic isotope fractionation*. California Institute of Technology. https://doi.org/10.7907/BWC2-RH54

Guo, W. (2020). Kinetic clumped isotope fractionation in the DIC-$H_2O$-$CO_2$ system: Patterns, controls, and implications. *Geochimica et Cosmochimica Acta*, *268*, 230–257. https://doi.org/10.1016/j.gca.2019.07.055

Guo, W., Mosenfelder, J. L., Goddard, W. A., III, & Eiler, J. M. (2009). Isotopic fractionations associated with phosphoric acid digestion of carbonate minerals: Insights from first-principles theoretical modeling and clumped isotope measurements. *Geochimica et Cosmochimica Acta*, *73*(24), 7203–7225. https://doi.org/10.1016/j.gca.2009.05.071

Guo, W., & Zhou, C. (2019a). Patterns and controls of disequilibrium isotope effects in speleothems: Insights from an isotope-enabled diffusion-reaction model and implications for quantitative thermometry. *Geochimica et Cosmochimica Acta*, *267*, 196–226. https://doi.org/10.1016/j.gca.2019.07.028

Guo, W., & Zhou, C. (2019b). Triple oxygen isotope fractionation in the DIC-$H_2O$-$CO_2$ system: A numerical framework and its implications. *Geochimica et Cosmochimica Acta*, *246*, 541–564. https://doi.org/10.1016/j.gca.2018.11.018

Hansen, M., Scholz, D., Froeschmann, M.-L., Schöne, B. R., & Spötl, C. (2017). Carbon isotope exchange between gaseous $CO_2$ and thin solution films: Artificial cave experiments and a complete diffusion-reaction model. *Geochimica et Cosmochimica Acta*, *211*, 28–47. https://doi.org/10.1016/j.gca.2017.05.005

Hill, P. S., Schauble, E. A., & Tripati, A. (2020). Theoretical constraints on the effects of added cations on clumped, oxygen, and carbon isotope signatures of dissolved inorganic carbon species and minerals. *Geochimica et Cosmochimica Acta*, *269*, 496–539. https://doi.org/10.1016/j.gca.2019.10.016

Hill, P. S., Tripati, A. K., & Schauble, E. A. (2014). Theoretical constraints on the effects of ph, salinity, and temperature on clumped isotope signatures of dissolved inorganic carbon species and precipitating carbonate minerals. *Geochimica et Cosmochimica Acta*, *125*, 610–652. https://doi.org/10.1016/j.gca.2013.06.018

Kele, S., Breitenbach, S. F., Capezzuoli, E., Meckler, A. N., Ziegler, M., Millan, I. M., et al. (2015). Temperature dependence of oxygen-and clumped isotope fractionation in carbonates: A study of travertines and tufas in the 6-95°C temperature range. *Geochimica et Cosmochimica Acta*, *168*, 172–192. https://doi.org/10.1016/j.gca.2015.06.032

Kelson, J. R., Huntington, K. W., Schauer, A. J., Saenger, C., & Lechler, A. R. (2017). Toward a universal carbonate clumped isotope calibration: Diverse synthesis and preparatory methods suggest a single temperature relationship. *Geochimica et Cosmochimica Acta*, *197*, 104–131. https://doi.org/10.1016/j.gca.2016.10.010

Kim, S.-T., & O'Neil, J. R. (1997). Equilibrium and nonequilibrium oxygen isotope effects in synthetic carbonates. *Geochimica et Cosmochimica Acta*, *61*(16), 3461–3475. https://doi.org/10.1016/s0016-7037(97)00169-5

Kluge, T., Affek, H. P., Dublyansky, Y., & Spötl, C. (2014). Devils Hole paleotemperatures and implications for oxygen isotope equilibrium fractionation. *Earth and Planetary Science Letters*, *400*, 251–260. https://doi.org/10.1016/j.epsl.2014.05.047

Kluge, T., John, C. M., Jourdan, A.-L., Davis, S., & Crawshaw, J. (2015). Laboratory calibration of the calcium carbonate clumped isotope thermometer in the 25-250°C temperature range. *Geochimica et Cosmochimica Acta*, *157*, 213–227. https://doi.org/10.1016/j.gca.2015.02.028

Leleu, T., Chavagnac, V., Delacour, A., Noiriel, C., Ceuleneer, G., Aretz, M., et al. (2016). Travertines associated with hyperalkaline springs: Evaluation as a proxy for paleoenvironmental conditions and sequestration of atmospheric $CO_2$. *Journal of Sedimentary Research*, *86*(11), 1328–1343. https://doi.org/10.2110/jsr.2016.79

Levitt, N. P., Eiler, J. M., Romanek, C. S., Beard, B. L., Xu, H., & Johnson, C. M. (2018). Near equilibrium $^{13}C$-$^{18}O$ bonding during inorganic calcite precipitation under chemo-stat conditions. *Geochemistry, Geophysics, Geosystems*, *19*(3), 901–920. https://doi.org/10.1002/2017gc007089

Marchitto, T., Curry, W., Lynch-Stieglitz, J., Bryan, S., Cobb, K., & Lund, D. (2014). Improved oxygen isotope temperature calibrations for cosmopolitan benthic foraminifera. *Geochimica et Cosmochimica Acta*, *130*, 1–11. https://doi.org/10.1016/j.gca.2013.12.034

McCrea, J. M. (1950). On the isotopic chemistry of carbonates and a paleotemperature scale. *The Journal of Chemical Physics*, *18*(6), 849–857. https://doi.org/10.1063/1.1747785

Mervine, E. M., Humphris, S. E., Sims, K. W., Kelemen, P. B., & Jenkins, W. J. (2014). Carbonation rates of peridotite in the Samail Ophiolite, Sultanate of Oman, constrained through $^{14}C$ dating and stable isotopes. *Geochimica et Cosmochimica Acta*, *126*, 371–397. https://doi.org/10.1016/j.gca.2013.11.007

Millero, F., Huang, F., Graham, T., & Pierrot, D. (2007). The dissociation of carbonic acid in NaCl solutions as a function of concentration and temperature. *Geochimica et Cosmochimica Acta*, *71*(1), 46–55. https://doi.org/10.1016/j.gca.2006.08.041

O'Neil, J. R., & Barnes, I. (1971). $C^{13}$ and $O^{18}$ compositions in some fresh-water carbonates associated with ultramafic rocks and serpentinites: Western United States. *Geochimica et Cosmochimica Acta*, *35*(7), 687–697. https://doi.org/10.1016/0016-7037(71)90067-6

O'Neil, J. R., Clayton, R. N., & Mayeda, T. K. (1969). Oxygen isotope fractionation in divalent metal carbonates. *The Journal of Chemical Physics*, *51*(12), 5547–5558. https://doi.org/10.1063/1.1671982

Parker, W. G., Yanes, Y., Surge, D., & Mesa-Hernández, E. (2017). Calibration of the oxygen isotope ratios of the gastropods *Patella candei crenata* and *Phorcus atratus* as high-resolution paleothermometers from the subtropical eastern Atlantic Ocean. *Palaeogeography, Palaeoclimatology, Palaeoecology*, *487*, 251–259. https://doi.org/10.1016/j.palaeo.2017.09.006

Sade, Z., Hegyi, S., Hansen, M., Scholz, D., & Halevy, I. (2022). The effects of drip rate and geometry on the isotopic composition of speleothems: Evaluation with an advection-diffusion-reaction model. *Geochimica et Cosmochimica Acta*, *317*, 409–432. https://doi.org/10.1016/j.gca.2021.10.008

Saenger, C. P., Schauer, A. J., Heitmann, E. O., Huntington, K. W., & Steig, E. J. (2021). How $^{17}O$ excess in clumped isotope reference-frame materials and ETH standards affects reconstructed temperature. *Chemical Geology*, *563*, 120059. https://doi.org/10.1016/j.chemgeo.2021.120059

Staudigel, P. T., & Swart, P. K. (2018). A kinetic difference between $^{12}C$-and $^{13}C$-bound oxygen exchange rates results in decoupled $\delta^{18}O$ and $\Delta_{47}$ values of equilibrating DIC solutions. *Geochemistry, Geophysics, Geosystems*, *19*(8), 2371–2383. https://doi.org/10.1029/2018gc007500

Swart, P. K., Lu, C., Moore, E. W., Smith, M. E., Murray, S. T., & Staudigel, P. T. (2021). A calibration equation between $\delta_{48}$ values of carbonate and temperature. *Rapid Communications in Mass Spectrometry*, *35*(17), e9147. https://doi.org/10.1002/rcm.9147

Tang, J., Dietzel, M., Fernandez, A., Tripati, A. K., & Rosenheim, B. E. (2014). Evaluation of kinetic effects on clumped isotope fractionation ($\Delta_{47}$) during inorganic calcite precipitation. *Geochimica et Cosmochimica Acta*, *134*, 120–136. https://doi.org/10.1016/j.gca.2014.03.005

Thiagarajan, N., Adkins, J., & Eiler, J. (2011). Carbonate clumped isotope thermometry of deep-sea corals and implications for vital effects. *Geochimica et Cosmochimica Acta*, *75*(16), 4416–4425. https://doi.org/10.1016/j.gca.2011.05.004

Tripati, A. K., Hill, P. S., Eagle, R. A., Mosenfelder, J. L., Tang, J., Schauble, E. A., et al. (2015). Beyond temperature: Clumped isotope signatures in dissolved inorganic carbon species and the influence of solution chemistry on carbonate mineral composition. *Geochimica et Cosmochimica Acta*, *166*, 344–371. https://doi.org/10.1016/j.gca.2015.06.021

Uchikawa, J., Chen, S., Eiler, J. M., Adkins, J. F., & Zeebe, R. E. (2021). Trajectory and timescale of oxygen and clumped isotope equilibration in the dissolved carbonate system under normal and enzymatically-catalyzed conditions at 25°C. *Geochimica et Cosmochimica Acta*, *314*, 313–333. https://doi.org/10.1016/j.gca.2021.08.014

Uchikawa, J., & Zeebe, R. E. (2012). The effect of carbonic anhydrase on the kinetics and equilibrium of the oxygen isotope exchange in the $CO_2$–$H_2O$ system: Implications for $\delta^{18}O$ vital effects in biogenic carbonates. *Geochimica et Cosmochimica Acta*, *95*, 15–34. https://doi.org/10.1016/j.gca.2012.07.022

Urey, H. C. (1947). The thermodynamic properties of isotopic substances. *Journal of the Chemical Society*, 562–581. https://doi.org/10.1039/jr9470000562

Usdowski, E., Michaelis, J., Bottcher, M., & Hoefs, J. (1991). Factors for the oxygen isotope equilibrium fractionation between aqueous and gaseous $CO_2$, carbonic-acid, bicarbonate, carbonate, and water (19°C). *Zeitschrift fur Physikalische Chemie-International Journal of Research in Physical Chemistry and Chemical Physics*, *170*, 237–249.

Wang, Z., Gaetani, G., Liu, C., & Cohen, A. (2013). Oxygen isotope fractionation between aragonite and seawater: Developing a novel kinetic oxygen isotope fractionation model. *Geochimica et Cosmochimica Acta*, *117*, 232–251. https://doi.org/10.1016/j.gca.2013.04.025

Wang, Z., Schauble, E. A., & Eiler, J. M. (2004). Equilibrium thermodynamics of multiply substituted isotopologues of molecular gases. *Geochimica et Cosmochimica Acta*, *68*(23), 4779–4797. https://doi.org/10.1016/j.gca.2004.05.039

Watkins, J. M., & Hunt, J. D. (2015). A process-based model for non-equilibrium clumped isotope effects in carbonates. *Earth and Planetary Science Letters*, *432*, 152–165. https://doi.org/10.1016/j.epsl.2015.09.042

Watkins, J. M., Hunt, J. D., Ryerson, F. J., & DePaolo, D. J. (2014). The influence of temperature, pH, and growth rate on the $\delta^{18}O$ composition of inorganically precipitated calcite. *Earth and Planetary Science Letters*, *404*, 332–343. https://doi.org/10.1016/j.epsl.2014.07.036

Watkins, J. M., Nielsen, L. C., Ryerson, F. J., & DePaolo, D. J. (2013). The influence of kinetics on the oxygen isotope composition of calcium carbonate. *Earth and Planetary Science Letters*, *375*, 349–360. https://doi.org/10.1016/j.epsl.2013.05.054

Wolthers, M., Nehrke, G., Gustafsson, J. P., & Van Cappellen, P. (2012). Calcite growth kinetics: Modeling the effect of solution stoichiometry. *Geochimica et Cosmochimica Acta*, *77*, 121–134. https://doi.org/10.1016/j.gca.2011.11.003

Yumol, L. M., Uchikawa, J., & Zeebe, R. E. (2020). Kinetic isotope effects during $CO_2$ hydration: Experimental results for carbon and oxygen fractionation. *Geochimica et Cosmochimica Acta*, *279*, 189–203. https://doi.org/10.1016/j.gca.2020.03.041

Zaarur, S., Affek, H. P., & Brandon, M. T. (2013). A revised calibration of the clumped isotope thermometer. *Earth and Planetary Science Letters*, *382*, 47–57. https://doi.org/10.1016/j.epsl.2013.07.026

Zeebe, R. E. (2020). Oxygen isotope fractionation between water and the aqueous hydroxide ion. *Geochimica et Cosmochimica Acta*, *289*, 182–195. https://doi.org/10.1016/j.gca.2020.08.025

Zeebe, R. E., Bijma, J., & Wolf-Gladrow, D. A. (1999). A diffusion-reaction model of carbon isotope fractionation in foraminifera. *Marine Chemistry*, *64*(3), 199–227. https://doi.org/10.1016/s0304-4203(98)00075-9

Zeebe, R. E., & Wolf-Gladrow, D. A. (2001). *$CO_2$ in Seawater: Equilibrium, Kinetics, Isotopes* (Vol. 65). Gulf Professional Publishing.

Zhang, J., Quay, P., & Wilbur, D. (1995). Carbon isotope fractionation during gas-water exchange and dissolution of $CO_2$. *Geochimica et Cosmochimica Acta*, *59*(1), 107–114. https://doi.org/10.1016/0016-7037(95)91550-d